OUKA
The University of Osaka
Institutional Knowledge Archive

Title	Impurity Spin Resonances in FeC12
Author(s)	Motokawa, Mitsuhiro
Citation	大阪大学, 1967, 博士論文
Version Type	VoR
URL	https://hdl.handle.net/11094/2612
rights	
Note	

The University of Osaka Institutional Knowledge Archive : OUKA

https://ir.library.osaka-u.ac.jp/

The University of Osaka

Impurity Spin Resonances in $FeCl_2$

Mitsuhiro Motokawa

Impurity Spin Resonances in $FeCl_2$

Mitsuhiro Motokawa

Abstract

Electron spin resonances of Fe^{3+} and Mn^{2+} ions in antiferromagnetic $FeCl_2$ were investigated at low temperatures using various microwaves under pulsed magnetic fields. Experimentall results show that these impurities in $FeCl_2$ occupy mainly the substitutional position and couple with host Fe^{2+} spins by considerably weak exchange interactions. Using a metamagnetic property of $FeCl_2$, these resonances were investigated both above and below the critical field H_c and the intralayer and interlayer exchange fields H_1 and H_2 upon these impurities were analysed as are given by

H_1 (AF) = 8.0 kOe H_2 (AF) = 4.2 kOe for Fe^{3+} spins,

H_1 (F) = 21.6 kO4 H_2 (AF) = 13.8 kOe for Mn^{2+} spins,

where AF and F mean the antiferromagnetic and ferromagnetic exchange interactions with Fe^{2+} spins, respectively.

We also investigated the ESR of interstitial Fe^{3+} impurity which lies between the Cl-Cl layers and found that the exchange interaction with neighboring Fe^{2+} spin is ferromagnetic. When the Mn^{2+} impurity concentration increases, Mn^{2+}-Mn^{2+} intralayer pair resonance could be observed and it was found that the pair coupling is ferromagnetic and weak (4kOe) compared with the Mn^{2+}-Fe^{2+} intralayer exchange interaction.

I. Introduction.

Much ~~Many~~ work~~s~~ on electron spin resonance experiments has ~~have~~ been done ~~studied~~ with developments of microwave techniques in several decades. Ferro- or antiferromagnetic resonance has also investigated by many researchers because it was very powerful to determine precisely the anisotropy energy of ordered magnetic materials, and most of main problems in ferro- or antiferromagnetic resonance have been solved satisfactorily. These works, however, concern with informations about motions of the net spins, i.e. those of spin waves as a whole spin system, and there are no report of the impurity spin resonance or the localized spin wave excitations in ferro- or antiferromagnetic materials. Generally speaking, it is difficult to observe the motions of impurity spins in ordered magnetic substances separating them from the net motion of host spins. Usually, one can observe only resonances of host spins slightly disturbed by the impurity spins accompanying with a small shift or a broadening effect of the resonance line width. But it is possible to observe the separated motion of impurity spins or impurity-localized spin waves without exciting the host spin system if magnetic characters of the host and impurity spins are considerably different from each other.
The theoretical treatments of this problem were discussed recently in the case of ferromagnetic impurity in ferro-

magnet,[1] antiferromagnetic one in ferromagnet[2] and ferro- or antiferromagnetic impurity in antiferromagnet[3] by calculating the localized spin wave modes arround the impurity.

We investigated the magnetic resonance of a single crystal of $FeCl_2$ containing a small amount of ferric ion by microwaves of the 35, 50 and 70 Gc/sec regions at liquid helium temperatures using a pulsed magnetic field up to 50 kOe, and several resonance lines having systematic frequency dependences were observed. Considering the frequency and angular dependences, absorption intensities and the temperature variation of the resonance lines, we concluded that these resonances came from the substitutional and interstitial Fe^{3+} impurity spins in $FeCl_2$, and reported as the first observation of such an electron spin resonance of impurity spin in metamagnetic substance.[4] It was shown that since the exchange interaction between impurity spins and host spins is sufficiently weak comparing with that of the host spins themselves, the impurity spins behave nearly freely as "paramagnetic" in the effective molecular field for the substitutional Fe^{3+} impurity. The intralayer and interlayer exchange interactions between Fe^{3+} spin and Fe^{2+} spins were determined by investigating both the antiferro- and ferromagnetic spin configurations of the host spin system under external magnetic fields.

On the other hand, spin resonance comes from the interstitial Fe^{3+} impurity was investigated recently and the exchange interaction between Fe^{2+} and the interstitial Fe^{3+} are estimated to be fairly strong and ferromagnetic.

Similar experiments have been done on single crystals of $FeCl_2$ mixed with isomorphous $MnCl_2$ (0.1 ~ 7.9 %), $CoCl_2$ (2 %) and $NiCl_2$ (2 %), and substitutional impurity spin resonances were observed for Mn^{2+} impurity but no resonance was observed for other mixtures. Moreover, it was found that specimens containing several percent of Mn^{2+} show a systematic line structure and it is attributed to the resonance which comes from Mn^{2+}-Mn^{2+} pairs in $FeCl_2$.

In this paper, a brief survey of the crystal structure of $FeCl_2$ and its magnetic properties are described in the next section, and the experimental techniques are mentioned in the section III. Experimental results and discussions are shown in the section IV dividing into four cases, namely

(1) Substitutional Fe^{3+} impurity spin resonance in $FeCl_2$,

(2) Substitutional Mn^{2+} impurity spin resonance in $FeCl_2$,

(3) Interstitial Fe^{3+} impurity spin resonance in $FeCl_2$,

(4) Substitutional Mn^{2+}-Mn^{2+} pairs in $FeCl_2$.

These experimental results and further discussions are summarized in the concluding remarks as will be shown in the last section.

II. Crystal structure and magnetic properties of $FeCl_2$.

The crystal structure of this compound is isomorphous with $CdCl_2$ having the hexagonal layer structure in which each layers of ferrous ions are separated by two layers of chlorine ions and its space group is D_{3d}^5-$R\bar{3}m$. The chlorine ions form nearly a cubic close-packed lattice and a ferrous ion lies at the center of an chlorine octahedron of which three fold axis coincides with the c-axis. The main part of a crystalline field, therefore, is of cubic symmetry and in addition to it, there is a trigonal crystalline field parallel to the c-axis arising from slight distortion of the octahedron. A ferrous ion has six nearest neighbor ferrous ions in the same layer and six next nearest neighbor ferrous ions in two adjacent layers. The lattice constants are determined to be a=3.58 $\mathring{A}$ * and c=17.54 $\mathring{A}$. Simplified models of the arrangements are shown in Fig.1 (a), (b) and (c). Other anhydrous chlorides such as $MnCl_2$,

---

* Recently the neutron research group[5] reported the spacing of $FeCl_2$ and a=3.60 $\mathring{A}$.

$CoCl_2$ and $NiCl_2$ are isomorphous with $FeCl_2$ having similar lattice parameters.

The magnetic properties of $FeCl_2$ has been first discussed by Landau[6] and the static magnetic measurements were performed by Starr, Bitter and Kaufmann,[7] Bizette et al.[8] and recently by Ono et al.[9] Theoretical treatments were done by Néel[10] and Kanamori,[11] and the antiferromagnetic properties of this crystal is now well known. There is a strong ferromagnetic exchange interaction among the intralayer ferrous ions, while the interlayer interaction is weak and antiferromagnetic. A strong uniaxial anisotropy favoring the c-axis is revealed by susceptibility and magnetization measurements and for this reason, $FeCl_2$ shows a antiferromagnetic-ferromagnetic transition, i.e. the metamagnetic transition, when an external magnetic field is applied along the c-axis and exceeds the critical field H_c. The neutron difraction investigation[5] supports this model. Schematic view of the spin configuration is shown in Fig. 2. Recently, Moessbauer study[12] and the precise magnetization measurements were done by Ono et al. who determined the ground state electronic structure of Fe^{2+} ion. They also show that the saturation value of magnetization is 4.35 μ_B and the most favourable value of the critical field H_c is 11.6 kOe. An example of the magnetization in $FeCl_2$ is illustrated in Fig. 3. Antiferromagnetic resonance of $FeCl_2$

single crystal was observed by Jacobs et al.[13] who showed the zero-field resonance energy to be 16 cm^{-1}. He also showed that the effective g-value of Fe^{2+} ion is about 4.0, assuming the ground state fictitious spin S=1. In our experiment, it is found that the critical field H_c shows a hysteresis under a pulsed magnetic field. As is shown in Fig.4, the critical field under an increasing field is 14 kOe whereas it shifts to 9.5 kOe when a decreasing field is applied.

III. Experimental Procedures.

(1) Preparation of specimens.

The single crystal of $FeCl_2$ and mixed crystals with $MnCl_2$, $CoCl_2$, and $NiCl_2$ were made from commercially available hydrates. The hydrated powders of these compounds were dehydrated in vacuum* with gradually increasing temperature up to 200°C for a week. The products of anhydrous ferrous chloride were re-heated in a pyrex tube up to 630°C to sublimate pure ferrous chloride in order to eliminate ferric chloride and oxychloride. The sublimed powder was then packed into a quartz ample and was sealed away in vacuum. After treatment the ample was kept in a furnace with a heat gradient of 25°C/cm at 750°C and then it was slowly cooled down

* Dry HCl gas was filled in the powder container several times for rapid and perfect dehydration.

to room temperatures taking about 48 hours. The obtained single crystal is brown and fairly transparent and easily crevabable along the c-plane.

In spite of these careful treatment of making single crystals, a small amount of Fe^{3+} impurity could not be rejected. According with the usual method of analytical chemistry, KCNS solution containing a little amount of HCI was used for testing Fe^{3+} ion and the result shows that it is inevitable to have the Fe^{3+} impurity of about 0.1 atomic percent[7] even in the best single crystal of $FeCl_2$. As will be shown in the next section, this fact is in good agreement with the resonance data concerning with the absorption intensity of the corresponding resonance lines. However, there is a difficult problem about the impurity states. Because of the charge neutrality principle in crystal, Fe^{3+} ion should accompany Fe^{2+} defect or excess Cl^- ion of which we have no information at present. Presumably the crystal contains both the Fe^{2+} defect and Fe^{3+} impurity and only a Fe^{3+} ion can act as a resonance center. Possible models of Fe^{2+} defect -Fe^{3+} coupled center will be discussed later. Other impurities such as 3d or 4f transition elements in pure as-grown crystal were also checked but there was no impurity except Fe^{3+} ion. For example, Cu^{2+} impurity was less than 0.01 %.

(2) Microwave equipments and cryostats.

Microwaves used for the experiment are in the frequency range of 35 ~ 90 Gc/sec. Usual experimental apparatus and techniques[14] were used to observe the resonances.

Cut view of the cryostat is shown in Fig. 5. The microwave transmission method was used for all frequency regions. German silver wave guide with a wall thickness of 0.3 mm was useful to prevent fast evaporation of liquid helium. Specimens were always immersed in the liquid helium bath in order to secure the precise temperature of the specimens. The microwave loss and frequency shift of the resonant cavity due to the filling up of liquid helium are practically negligible.

A pulsed magnet coil is placed at the bottom of the liquid helium dewar bessel as is shown in Fig. 5. Vertical pulsed field was applied to the resonant cavity so that it was necessary to rotate the specimen perpendicularly to the pulsed field axis to get the angular dependence of the resonance pattern. The mechanism of this rotational method is illustrated in Fig. 6.

(3) Generation of high pulsed magnetic fields.

There has been a growing interest in the production and use of high magnetic fields for several decades and it would not be necessary to show here the general process of producing the pulsed fields. The state of high field

production and current reseach activities have been summarized at the International Conference in High Magnetic Fields.[15]

An Application of the pulsed fields to antiferromagnetic resonance was first performed by Foner[16] [17] [18] who observed the resonance in Cr_2O_3 and in its mixed crystals with Al_2O_3. As there are several differences and new developments in the production and measurement of pulsed fields compared with the Foner's work, we show our experimental procedure comparing with his one.

The block diagram of the experiment is illustrated in Fig. 7. Electrolytic condensors of 500 volt and 3000 μF were used for the energy bank of the magnetic fields which was produced by discharging through Sendaitron, a kind of laboratory ignitron developed at Tohoku University. Use of the electolytic condensor is generally not desirable because it is weak when applied voltage is transiently reversed. But as the Sendaitron is a sharp one-way tube, there is no oscillational current in the coil and condensor system and any serious accidents could not be anticipated. Merits of using electrolytic condensor are low cost and compactness of the condensor bank.

Making the first impulse from a push button, two pulses are generated by the monostable multivibrator and interval of two pulses can be controled from 1 to 100 μ

seconds. The first pulse triggers the synchroscope or the memoriscope and the second pulse is used for the triggering of the pulsed magnetic field. Such two pulse system is convenient to see the early stage of magnetic fields and associated resonance phenomena. On the other hand, the delaying unit of the synchroscope can be used of one wishes to see the later stage of the pulsed field and the related resonances.

We made several coils for generating suitable pulsed magnetic fields and a typical example of coil data is as follows: $L=322.6\ \mu H$, $R_{300^oK}=1.403\ \Omega$, $R_{4.2^oK}=0.087\ \Omega$, inner diameter is 8 mm, coil length is 30 mm with 60×5 turns of Cu wire (diameter=0.5 mm), the maximum current is 2000 A which produces the maximum magnetic field of 110 kOe with the field uniformity of $5\ 10^{-3}$/cm both along the coil axis and in the coil plane. The pulse duration time is about 4.0 msec. It should be mentioned that if one wishes to have very strong fields more than 500 kOe, beryllium-copper helix developed by Foner and Kolm[18] may be necessary. However, the field uniformity in such helical layer coil may not be so high that we may not be able to observe a sharp resonance line sush as that of DPPH, a standard specimen for paramagnetic resonance. The coil is immersed in the liquid helium bath to keep very low electrical resistivity. The field homogenuity

in the coil was measured in the following way: two pieces of small DPPH were located in the resonant cavity separately to one another keeping a distance of $5 \sim 10$ mm and then a pulsed field was applied. Consequently, one observes two peaks of each resonance lines separately if the local fields at two DPPH specimens were different. Moving the resonant cavity in the coil, we can obtain the field distribution and its homogenuity with high accuracy.

A pick up coil and the compensation coils were wound inside the pulsed field coil to observe the change of magnetization at critical field. As is shown in Fig. 8, two compensation coils with a variable resistor were used to reject large flux change of the main coil. In this system, both magnetic resonance and magnetization are observable at the same time and this method is very useful to examine the relation between the magnetic resonance and magnetic structure of such a metamagnetic substance.

Now let us discuss briefly a relation between the resonance line width and the band width of the receivers. There is no consideration about this problem but it is important to have a sharp resonance line as a transient phenomena. As is well known, there is a relationship between a signal frequency and a cut off frequency of the transmission line. We assume that the imput magnetic resonance signal can be described by a gaussian form as

a function of time.* Of course the band width depends on the sweep velocity of the external pulsed magnetic field. Denoting the imput signal voltage to be $E=E_0\exp(-\alpha t^2)$, where α being a constant, we can calculate the cut off frequency of the transmission line using usual techniques of electrical engineering and the result shows that the cut off frequency f_c is calculated to be $f_c=3f_n$ where f_n is the nominal cut off frequency which is written by $f_n=(1/2)\sqrt{\alpha/\pi}$. Fig. 9 shows the relation between the cut off frequency and the sweep velocity of the pulsed magnetic fields. Three lines corresponds to the cases where the resonance line widths are 1 Oe, 10 Oe and 100 Oe, respectively. Accordingly, it is easily obtained from Fig. 9 that the band width of the amplifier system is required to be 5 Mc/sec if we have to observe the resonance of 10 Oe in the line width when we use our pulse coil.

Finally let us consider the ultimate sensitivity of the pulsed magnetic field ESR spectrometry. Sensitivity considerations under a static magnetic field has been done by Feher[19] who showed that the minimum spin numbers N_{min} to be detectable by an ideal ESR spectrometer are $\sim 10^{11}$ spins under an usual experimental condition. In

---

* If necessary, one can easily extend this discussion for other line shapes.

pulsed field resonance, however, it is impossible to have this value because of the necessity of wide band width in the amplifier system. Considering a relation $N_{min} \propto \Delta H \sqrt{f}$ where ΔH is the resonance line width and f represents the band width of the transmission line, we have the ultimate sensitivity of the minimumdetectable spin number $N_{min} \sim 10^{15}$. Of course this value is an ideal one and the practical value may be of the order of $\sim 10^{15 \sim 16}$ spins if we use a superheterodyne receiver system. Consequently it is possible to observe electron spin resonance from highly diluted paramagnetic impurities in crystals and liquids as well as ferro- or antiferromagnetic resonances and impurity spin resonance in $FeCl_2$.

IV. Experimental results and discussions.

(1) Fe^{3+} impurity spin resonance in $FeCl_2$.

Several resonance lines were observed in "pure" $FeCl_2$ at each frequency range when an external magnetic field was applied along the c-axis at liquid He temperatures. The frequency-field diagram of the resonance points is shown in Fig. 10. At 45 Gc/sec, for example, resonance absorptions were observed at 2kOe and 12 kOe in antiferromagnetic state and 27, 33 and 39 kOe in ferromagnetic state. Fig. 11 shows the absorption line shapes in antiferromagnetic

state. The line widths are about 1.2 kOe for the lowest field resonance and 2 or 3 kOe for three resonances in ferromagnetic state. For the resonance which occurs near the critical field (the branch III), the width is not clear because the absorption intensity is very weak comparing with those of the other resonances. There are six branches having a linear frequency dependence as is shown in Fig. 10 and the effective g-value is 2 for each branch except the branch III which acrosses the origin. Two low field branches (branch I and II) converge to 42 Gc/sec at zero field and the branch IV in the ferromagnetic state bisects the abcissa at 17 kOe. There are two side lines V and VI, both of them are parallel to the branch IV. Angular dependences of these resonance lines were investigated mainly in the antiferromagnetic state. The resonance field corresponding with the branch I shows monotonic increasing when an external field declines from the c-axis. However, the branch III shows a rapid decreasing when an angle between the c-axis and the magnetic field increases. An example of the angular dependences is shown in Fig. 12. Most of these experimental data were obtained at 1.1°K. These absorption lines were very difficult to observe above 4.2°K.

Now let us consider the origin of these resonance lines. It is obvious that these resonance lines do not correspond with those of the antiferromagnetic resonance

because the usual antiferromagnetic resonance frequency comes to the far- infrared frequency region as Jacobs et al.[13] pointed out. Of course these resonances are not explained by paramagnetic or ferromagnetic resonances. Considering these fact, we tried to analyze these lines by an impurity spin resonance model comes from Fe^{3+} spins in $FeCl_2$.

Consider the Fe^{3+} impurity spins in the Fe^{2+} layers as are shown in Fig. 13(a). We assume that both the intra-layer and interlayer exchange interactions between Fe^{3+} and Fe^{2+} spins are antiferromagnetic and are expressed by the effective fields H_1 and H_2, respectively. The theory of superexchange interaction[20] predicts that H_1 and H_2 may be much smaller than the exchange field between the intralayer ferrous spins. Moreover, the anisotropy energy of Fe^{3+} ion is very small compared with that of Fe^{2+} ion. Under such conditions the Fe^{3+} spin may easily be able to move independently. It should be noticed that there are three cases to be discussed of the resonance conditions of Fe^{3+} spins when the external magnetic field H_0 is applied along the c-axis. Noticing the presence of the metamagnetic critical field H_c(11.6 kOe), one can obtain the resonance conditions as follows, where $H_1 > H_2$ and $H_1 - H_2 > H_c$ are assumed so as to explain the experimental results.

(a) $H_0 < H_c$.

There are two inequivalent impurity spins in this case

as are shown in Fig. 13(a). The type-1 spin points in the direction opposite to the external field while the type-2 spin is parallel to H_0 so that the resonance conditions for both spins can be obtained as follows:

$$\omega/\gamma = H_1 - H_2 - H_0 \quad \text{for type 1,} \tag{1}$$

$$\omega/\gamma = H_1 - H_2 + H_0 \quad \text{for type 2,} \tag{2}$$

where γ is the effective gyromagnetic ratio of Fe^{3+} spins in $FeCl_2$. Assuming g=2.00 and H_1-H_2=14.6 kOe, theoretical curves are drawn as are shown in Fig. 10 which shows remarkable coincidence with the experimental results.

(b) $H_c < H_0 < H_1+H_2$.

As is shown in Fig. 13(b), there are no inequivalent spins in this case because of the ferromagnetic arrangement of the host spin system. Noticing the sign of H_2, the resonance condition can be written as

$$\omega/\gamma = H_1 + H_2 - H_0. \tag{3}$$

The theoretical line is shown in Fig. 10 but there is no experimental point.

(c) $H_0 > H_1+H_2$.

In this case the impurity magnetic moment points parallel to the magnetic field and the resoance condition is

$$\omega/\gamma = H_0 - (H_1 + H_2). \tag{4}$$

The theoretical line shown in Fig. 10 coincides fairly well with the experimental result if we take the effective field H_1+H_2 to be 17 kOe. Comparing this value with H_1-H_2 in the case (a), we have

$$H_1 = 15.8 \text{ kOe}, \quad H_2 = 1.2 \text{ kOe}. \tag{5}$$

It should be noted that the experimental result could not be explained if one assumed a ferromagnetic H_1 or H_2.

It should be noticed that H_1 and H_2 do not come from the exchange interaction only but the dipolar field between Fe^{2+} and Fe^{3+} spins should be taken into account. The dipolar field in this crystal has been already discussed by Kanamori[11] who divided it into three parts: The first is the field arising from the magnetic moments within the Lorentz sphere, the second the Lorentz field, and the third the demagnetization field comes from macroscopic surface. The total dipolar field acting on substitutional impurity spin belonging to the + sublattice is given by

$$H_{dip} = \phi_1 M^+ + \phi_2 M^- + (4\pi/3)(M^+ + M^-) - \hat{N}(M^+ + M^-), \tag{6}$$

where ϕ_1 and ϕ_2 are the diagonal tensors obtained from the dipole sum within the Lorentz sphere, $\hat{N}$ is the demagnetization tensor, and M^+ and M^- are the magnetization of the sublattice per c.c. The magnitudes of ϕ_1 and ϕ_2 have been

also calculated as

$$\phi_1{}^z = -21.9 \qquad \phi_2{}^z = 8.37 \qquad (7)$$

For the impurity spin of the - sublattice, ϕ_1 and ϕ_2 should be interchanged

In our experiments, both the nearly spherical and thin disk form specimens are tested. Examples of the shape dependence will be shown in the Mn^{2+} resonance line later. The experimental data shown in Fig. 10 are of the spherical specimen so that Lorentz field term and demagnetization part in Eq.(6) cancels to each other. Using the calculated value of $M^{\pm} = g\mu_B\langle S_z\rangle = 357$ Oe/c.c., the dipolar contribution to the effective fields H_1 and H_2 can be calculated as

$$H_{dip\ 1} = -7.83 \text{ kOe}, \qquad H_{dip\ 2} = -2.95 \text{ kOe}. \qquad (8)$$

Then the exchange fields acting on the Fe^{3+} impurity can be calculated as follows:

$$\begin{aligned} H_1 &= H_{ex\ 1} - H_{dip\ 1}, \\ H_2 &= H_{ex\ 2} + H_{dip\ 2}, \end{aligned} \qquad (9)$$

where $H_{ex\ 1}$ and $H_{ex\ 2}$ mean the intra- and interlayer exchange fields upon the Fe^{3+} ion, respectively. Using Eqs.(5), (8) and (9), one can obtain as

$$H_{ex\ 1}(AF) = 8.0 \text{ kOe}, \qquad H_{ex\ 2}(AF) = 4.2 \text{ kOe}.$$

Thus the exchange interaction between the Fe^{3+} and Fe^{2+} spins are determined perfectly.

Now we have two problems. The first of them is that there are still unexplained resonance lines observed in Fig. 10. The branches I, II and IV can be explained satisfactorily but there remain three branches. Of these unexplained branches, the branch III can be explained as the interstitial Fe^{3+} resonance line as will be discussed later. So the branch V and VI remain to be unsolved. These lines might come from more complex centers accompanying with Fe^{2+} defect, or substitution of O^{2-} for Cl^-. ~~Possible models of these centers can be considered as are shown in Fig. 14.~~ However there is no evidence whether these centers are actually possible or not. It should also be noticed that our resonance data cannot show about the transfer motion of Fe^{3+} in the crystal.

The second problem is as follows: The experimental results show the effective g-value is 2.0 within the experimental error. Generally speaking, however, it is not necessary to be g=2.0 for such an impurity spin resonance because the impurity spin interacts with the surrounding host spins which might produce the g-shift. Accordingly, it is necessary to estimate the expected g-shift of Fe^{3+} spin in $FeCl_2$. Recently, localized spin waves and their g-values have been calculated theoretically by several researchers.(1)(2)(3) In the case of Fe^{3+} spins in $FeCl_2$, however, the impurity

is so "paramagnetic" that a model of "collective" spin wave motion around the impurity may not be necessary. Moreover, we should take into account both the intralayer and interlayer neighboring ferrous spins as a surrounding spin system, which is not so easy to analyze thoroughly. Considering these facts, we tried to calculate the effective g-value of a spin-cluster system in which a central spin S_o corresponding with the Fe^{3+} spin couples with several type 1 spins by J_1 and with type 2 spins by J_2, where J_1 and J_2 represent intralayer and interlayer exchange interactions, respectively. Adding to the external field, effective fields H_{E1} and H_{E2} for the 1 and 2 spins are assumed as the resultant molecular and anisotropy fields acting on the neighboring 1 and 2 spins. An effective spin Hamiltonian of the spin-cluster system can be written as

$$\begin{aligned} H = {} & g_o\mu_B H_o S_o^z + g_1\mu_B \sum_{intra} S_1^z(H_o+H_{E1}) \\ & + g_2\mu_B \sum_{inter} S_2^z(H_o+H_{E2}) + 2J_1 S_o \sum_{intra} S_1 \\ & + 2J_2 S_o \sum_{inter} S_2, \end{aligned} \tag{10}$$

where μ_B is the Bohr magneton and the summations take each nearest neighbor ferrous spin into account. For simplicity S=1/2 and $g_1=g_2$ are assumed to solve the problem. Noticing the fact that $H_{E1} \sim H_{E2}$ and that both are large enough compared with H_o, J_1 and J_2, one can calculate the

energy splitting corresponding to S_o spin flopping, and we have a deviation of the effective g-value of the S_o spin to be

$$\Delta g = \frac{g_1 - g_a}{g_o} \cdot \left\{ \frac{N_1 J_1{}^2}{(g_1 \mu_B H_{E1})^2} + \frac{N_2 J_2{}^2}{(g_1 \mu_B H_{E2})^2} \right\}, \qquad (11)$$

where N_1 and N_2 show the numbers of nearest neighbor 1 and 2 spins. Evaluating Eq.(11), $\Delta g \lesssim 10^{-3}$ is obtained which does not contradict experiment.

An introduction of the Hamiltonian expressed by Eq.(10) corresponds with a more precise treatment of the simple calculation of the resonance conditions leading to Eqs. (1)-(4). It is easily calculated that Eqs.(1)-(4) are still applicable if we take H_1 and H_2 as follows:

$$H_1 = N_1 J_1 \left(1 + \frac{J_1}{g_1 \mu_B H_{E1}} \right), \qquad (12)$$

$$H_2 = N_2 J_2 \left(1 + \frac{J_2}{g_1 \mu_B H_{E2}} \right). \qquad (13)$$

The correction terms $J_1/g_1\mu_B H_{E1}$ and $J_2/g_1\mu_B H_{E2}$ are of the order of 10^{-2} so that H_1 and H_2 may practically be considered as $N_1 J_1$ and $N_2 J_2$, respectively.

(2) Mn^{2+} impurity spin resonance in $FeCl_2$.

Similar experiments were performed on the Mn^{2+} impurity in $FeCl_2$ with varing Mn^{2+}-concentrations. There are two

merits of Mn^{2+} resonance in $FeCl_2$ copared with that of Fe^{3+} spins. One of them is that Mn^{2+} can be considered as the substitutional impurity without any defects and the other is the easiness of controling the impurity concentration. A typical pattern of resonance absorption for the specimen which contains 1.5 % Mn^{2+} at 85 Gc/sec and 1.5°K with the external field parallel to the c-axis is shown in Fig.15. Two resonance absorptions were observed at 5 and 20 kOe and each resonance occurs at the antiferromagnetic and ferromagnetic states, respectively. The line widths are 0.8 kOe for the lower field resonance and 1.4 kOe for the higher one. The absorption intensities are proportional to the concentration rate of Mn^{2+} impurity as is shown in Fig.16, which was measured by comparing with that of Mn-tutton salt. The resonances were observed in all frequency ranges at 1.5°K and the frequency-field diagram is illustrated in Fig.17. Two low field branchs(branch I and II) converge to 69 Gc/sec at zero field and the high field branch (branch III) bisects the abcissa at -3 kOe if one extraporate the line to low field side. As in the case of Fe^{3+} rrsonance, the relation between the resonance fiels and the frequency is linear and the effective g-value is equal to 2. Fig.18 shows the temperature dependence of absorption intensity at 45 Gc/sec, which decreases with increaseing temperature more rapidly than 1/T in usual

paramagnetic resonance and resonance line disappears near $10^{\circ}K$. Within the experimental error, the line width does not change with varing temperature but resonance points shift slightly to low field side with increasing temperature. As is shown in Fe^{3+} in $FeCl_2$, the intra- and interlayer effective field H_1 and H_2 can be calculated from the experimental result as are given by

$$H_1 = 13.8 \text{ kOe}, \quad H_2 = 10.8 \text{ kOe}, \tag{14}$$

and the exchange field was obtained by reducing the dipolar effect as

$$H_{ex\ 1}(F) = 21.6 \text{ kOe}, \quad H_{ex\ 2}(AF) = 13.8 \text{ kOe}. \tag{15}$$

It is interesting that the intralayer Mn^{2+}-Fe^{2+} exchange interaction is ferromagnetic. Models of the impurity states are shown in Fig.19.

The angular dependences of resonance points in antiferromagnetic state were measured at $1.5^{\circ}K$ using microwaves of 45, 65 and 85 Gc/sec and is shown in Fig.20. All resonance fields increase with inclining the external field from the c-axis. The angular dependence illustrated in Fig.20 can be explained as follows: The effective field responsible to the resonance frequency is the resultant field given by $\vec{H}_o+\vec{H}_1+\vec{H}_2$. Since $\vec{H}_1+\vec{H}_2$ points parallel to the c-axis, the resonance frequency ω can be calculated

as

$$\omega/\gamma = \sqrt{H_o^2 + (H_1 + H_2)^2 + 2H_o(H_1 + H_2)\cos\theta} \qquad (16)$$

where θ is the angle between the c-axis and H_o. Full lines in Fig.20 are drawn by the formula Eq.(16) which show satisfactory agreement with the experimental data.

(3) Interstitial Fe^{3+} impurity spin resonance in $FeCl_2$.

As was discussed previously, the resonance branch III in Fig.10 shows somewhat different properties compared with those of the branches I, II and IV. The absorption intensity is very weak and the effective g-value is not equal to 2.0 but shows $g^*=2.4$ when H_o is parallel to the c-axis. Moreover the angular dependence is quite different as is shown in Fig.12. If the branch III comes from any substitutional impurity, the angular dependence should be expressed by the curves as are typically shown in Fig.20, because the effective mokecular fields acting on the impurity is always nearly parallel to the c-axis. To explain such peculiar properties of the branch III resonance, we assumed the presence of an interstitial Fe^{3+} impurity spin between the Cl-Cl layers. Of course it may be impossible to have an isolated Fe^{3+} interstitial impurity in the crystal because of the charge neutrality principle. Perhaps ~~it may occur frequently that a Fe^{2+} regular ion~~ Fe^{3+} ion may be at

~~jumps to~~ the interstitial site accompanying with a Fe^{2+} defect in the regular position or substitution of O^{2-} for Cl^- ~~and a part of these randomly appeared Fe interstitial atom changes to Fe^{3+} ion.~~ This model is not inconsistent with the fact that the branch III resonance becomes weak and diminishes finally when a single crystal of as-grown $FeCl_2$ is annealed enough. The proposed model of the interstitial Fe^{3+} ion is shown in Fig.21(a).

To discuss the electron spin resonance of such an impurity, the following simplified model is assumed. Suppose a three spin system S_o, S_1 and S_2 corresponding with the interstitial and two nearest neighbor interlayer spins, respectively. This simplified model is given in Fig.21(b). Assuming each spins to be S=1/2, the following effective spin Hamiltonian is introduced, namely,

$$H = g_o\mu_B\vec{H}_o\vec{S}_o + g_1\mu_B\vec{H}_o(\vec{S}_1 + \vec{S}_2) + g_1\mu_B(\vec{H}_{E1}\vec{S}_1 + \vec{H}_{E2}\vec{S}_2) + 2J\vec{S}_o(\vec{S}_1 + \vec{S}_2), \qquad (17)$$

where simbols are shown in Fig.21(b), and the first and second terms are Zeeman energies, the third term means the effective molecular field enrgy acting on the neighboring S_1 and S_2 spins and an isotropic exchange interaction is assumed between S_o and S_1+S_2 as is giben by the last term. Now it is assumed that the terms concerning with H_{E1}^z, H_{E2}^z and J are large enough compared with other terms. Then the perturbation calculation is possible after diagonalizing H_{E1}^z, H_{E2}^z and J terms. Effect of the x-components of $\vec{H}_{E1}$

and $\vec{H}_{E2}$ can be calculated by the usual tratment of the theory of antiferromagnetism.[21] As the result, the resonance character corresponding the spin flopping of the central spin S_o can be described by the effective g-tensor as is given by

$$\begin{aligned} g_{//} &= (1 - 2c_1^2)g_o + 2c_1^2 g_1 \\ g_{\perp} &= (1 - c_1^2)g_o + 2c_1 c_2 g_1 \end{aligned} \tag{18}$$

where c_1 and c_2 are parameters representing the mixing ratio of the spin functions. Considering the experimental result ($g_{//} = 2.4$), c_1 is determined as

$$c_1 = 0.32, \tag{19}$$

where g_1=4.0 is used.[13] The value of $g_{\perp}$ is determined as $g_{\perp}$=10 so as to explain the experimental result as is shown in Fig.22. This means that c_2 should be as

$$c_2 = 4.0. \tag{20}$$

Considering these values of c_1 and c_2, we can estimate the exchange interaction J as

$$J(F) \sim 20 \text{ cm}^{-1} \tag{21}$$

where $H_{EX}^{z} \sim 10 \text{ cm}^{-1}$ and H_A (anisotropy field energy of Fe^{2+} spin) $\sim 20 \text{ cm}^{-1}$ are taken into account according to the

antiferromagnetic resonance data.[13] This shows the exchange interactions between the interstitial Fe^{3+} spin and neighboring Fe^{2+} spins are ferromagnetic and fairly strong.

*Cont. on the next page.

(4) Mn^{2+}-Mn^{2+} pair resonance in $FeCl_2$.

Recently we found that several sets of resonance lines are newly observed when Mn^{2+} concentration increases in $FeCl_2$. Roughly speaking, these new lines seem to be hyperfine structure of main Mn^{2+} resonance although separations are too wide. Several examples are shown in Fig.23. The experimental features are summalized as follows: The number of resonance lines are 4 or 5 including the Mn^{2+} main line but the relative absorption intensity is not equivalent and varies with varing temperature. Fig.23(a) shows the absorption lines observed at 4.2°K using 45 Gc /sec microwave. When temperature decreases down to 1.5°K, the absorption ratio of each resonance lines changes as are shown in Fig.23(b). Temperature dependence of the absorption intensity is shown in Fig.24, and the frequency-field diagram of these lines is illustrated in Fig. 25. These new lines are explained by weakly coupled Mn^{2+}-Mn^{2+} intralayer pair model in $FeCl_2$. ~~The effective spin Hamiltonian for this case is given by~~

$$\mathcal{H} = g\mu_B \left\{ \vec{H}_1 - (1/6)\vec{H}_1 + \vec{H}_2 \pm \vec{H}_0 \right\} \left(\vec{S}_1 + \vec{S}_2 \right)$$

We do not discuss here in details.

*On the other hand, the theory of superexchange interaction predicts that the 180°-interaction[20] may be dominant for such an interstitial Fe^{3+} spin considering the crystal symmetry, and suggests that the exchange interaction between Fe^{2+} and Fe^{3+} spin is antiferromagnetic. This fact is against with our model, but it is difficult to determine the path and sign of the superexchange interaction at present.

~~lar contribution can be calculated as $H_{p\ dip}$=0.4 kOe and the exchange contribution is estimated to be ferromagnetic and $H_{p\ ex}$=2.0 kOe. The sign of the exchange energy was determined by temperature dependence of absorption intensity ratio of observed structures.~~

V. Concluding discussions.

(1) Review of the experimental results.

We have discussed about various kinds of impurity spin resonances observed in $FeCl_2$ at low temperatures. The important point to be able to observe such an impurity spin resonance in an ordered magnetic material is that the impurity spin couples weakly to the host spin system and the anisotropy energy should be different from each other. Accordingly these impurity resonance are not always obserbable in ferro- or antiferromagnetic crystals. As $FeCl_2$ is an Ising-like spin system, these resonances were observed fortunately. We also tried to observe other impurities such as Co^{2+} and Ni^{2+}but there was no resonance corresponding to these impurities. It may be also interesing to change the host crystal. For example, impurity spin resonance in $FeBr_2$ may be also interesting.

(2) The superexchange interaction of impurity spins.

We consider briefly here the reason why the intralayer exchange interactions between Fe^{3+} or Mn^{2+} and host Fe^{2+} spins are reversed in sign, and why the resonance absorption could not be observed in the case of Co^{2+} and Ni^{2+} impurity. The properties of impurity spins in $FeCl_2$ are concerned to the superexchange interactions of pure anhydrous chloride of these atoms, i.e. $FeCl_3$, $MnCl_2$, $CoCl_2$ and $NiCl_2$, which were treated theoretically in details by Kanamori.[20] According to his theory, the total exchange interaction will decrease with decreasing number of 3d electrons for Fe^{3+} or Mn^{2+} taking several possible exchange paths into account and the sign is uncertain while the strong ferromagnetic superexchange interaction exists in the case of Ni^{2+}. Co^{2+} and Fe^{2+} are considered to be similar as Ni^{2+} from thir electronic configurations. These facts are strongly related to their ordering temperatures (see Table 1) and the spin structures determined by neutron difraction measurements,[5][22] that is, the Néel temperature of $MnCl_2$ is lower than those of other chlorides by a factor about 1/10 and $MnCl_2$ has very complicated spin structure in which there are both intralayer ferro- and antiferromagnetic couplings of Mn^{2+} spins forming domains. Similar conditions are also expected for these spins in $FeCl_2$, and explain our experimental results qualitatively. Fe^{3+} or Mn^{2+} impurity in $FeCl_2$ couples with surrounding Fe^{2+} spins

through weak interaction of which sign may be reversible easily by slight diference of circumstances, for instance, local distortion of lattices because of diference of the ion radius or excess charge of Fe^{3+}. On the other hand, the spins such as Co^{2+} or Ni^{2+} couple with Fe^{2+} strongly, and they are no longer regarded as "paramagnetic spin". The resonance frequencies of these ions are estimated to be considerably high and they may lie in a spin wave band of host spins, so that this fact makes impossible to observe the resonance absorptions of Co^{2+} and Ni^{2+} impurities.

Acknowledgements

The auther wishes to express his sincere thanks to Prof. M.Date for his guidance throughout this work. He is also indepted to Prof. K.Ono for his offering samples in the early stage of this work and to Prof. J.Kanamori for his helpful discussions on superexchange interaction. He is grateful to Mr. M.Mitani who initially developed the pulsed field resonance techniques in our laboratory.

References

(1) T. Wolfram and J. Callaway, Phys. Rev. 130 (1963) 2207.
S. Takeno, Prog. Theor. Phys. 30 (1963) 731.
Li Yin-Yuan and Zhu Yan-Qing, Acta Phys. Sinica 19 (1963) 753.

(2) H. Ishii, J. Kanamori and T. Nakamura, Prog. Theor. Phys. 33 (1965) 795.

(3) T. Tonegawa and J. Kanamori, Phys. Letters 21 (1966) 130.

(4) M. Date and M. Motokawa, Phys. Rev. Letters 15 (1965) 854.

(5) M. K. Wilkinson, J. W. Cable, E. O. Wollan and W. C. Koehler, Phys. Rev. 113 (1959) 497.

(6) L. Landau, Phys. Z. Sowjet, 4 (1933) 675.

(7) C. Starr, F. Bitter and A. R. Kaufmann, Phys. Rev. 58 (1940) 977.

(8) H. Bizette, C. Terrier and B. Tsai, Comptes Rendus 243 (1956) 895, 1295.

(9) A. Ito and K. Ôno, J. Phys. Soc. Japan 20 (1965) 784.

(10) L. Néel, Comptes Rendus 242 (1956) 1549.

(11) J. Kanamori, Prog. Theor. Phys. 20 (1958) 890.

(12) K. Ôno, A. Ito and T. Fujita, J. Phys. Soc. Japan

19 (1964) 2119.

(13) I. S. Jacobs, S. Roberts and P. E. Lawrence, J. appl. Phys. 36 (1965) 1197.

(14) M. Date, J. Phys. Soc. Japan 16 (1961) 1337.

(15) H. Kolm, High Magnetic Field, MIT Press and Wiley (1962).

(16) S. Foner, Le J. De Phys. Et Radium 20 (1959) 336.

(17) S. Foner, Phys. Rev. 107 (1957) 683.

(18) S. Foner and H, Kolm, Rev. Sci. Inst. 27 (1956) 547.

(19) G. Fehr, Bell System Tech. J. 36 (1957) 449.

(20) J. Kanamori, J. Phys. Chem. Solid 10 (1959) 87.

(21) T. Nagamiya, K. Yosida and R. Kubo, Advances in Physics vol.4 (1955)

(22) M. K. Wilkinson, J. W. Cable, E. O. Wollan and W. C. Koehler, Semiannual Progress Report, ORNL-2430 Sept. 10 (1956) 65.

Figure Captions.

Fig. 1. Crystal structure of $FeCl_2$.

(a) Layer structure of $FeCl_2$.

A, B, and C show the types of packing.

(b) A unit octahedron.

(c) Intralayer nearest neighbors and next nearest neighbors in adjacent layers.

Fig. 2. Spin arrangements of $FeCl_2$ in (a) antiferromagnetic state and (b) ferromagnetoc state.

Fig. 3. Magnetization of $FeCl_2$ when a static magnetic field is applied along the c-axis. Demagnetization effect is corrected. After Ôno et.al.[9]

Fig. 4. Magnetization of $FeCl_2$.

(a) Deferential curve of magnetization when a pulsed magnetic field is applied to the c-axis. The abcissa is time and the curve increasing and decreasing gradually with time indicates the change of the intensity of the magnetic field. The another is the change of magnetization with increasing and decreasing field.

(b) Detailed curve of (a) with increasing field.

(c) Magnetization integrated from (a). Large hysteresis effect is shown in H_c. Demagneti-

zation effect is not corrected.

Fig. 5. Cut view of the cryostat.

Fig. 6. Schematic view of the rotating specimen holder which is made of polystylene and is inserted in the microwave cavity.

Fig. 7. Block diagram of the measureing system to observe magnetic resonances using pulsed magnetic field.

Fig. 8. Schematic view of a pick up coil and compensation coils wound inside the pulsed field coil.

Fig. 9. A nomograph of the relation between the cut off frequency f_c of the detecting system (amplifier and synchroscope) and the sweep velocity of pulsed magnetic field.

Fig.10. Frequency-field diagram of Fe^{3+} resonances. Solid lines except branch III are the theoretical lines in accord with Eqs.(1) - (4).

Fig.11. The absrption curve of Fe^{3+} resonances at 45 Gc/sec and 1.5°K. A small absorption near the critical field appears with only increasing field because of the hysteresis effect of $FeCl_2$.

Fig.12. Angular dependence of Fe^{3+} resonance points in antiferromagnetic state of $FeCl_2$.

Fig.13. Spin arrangements of Fe^{3+} spin in $FeCl_2$.

Fig.14. Possible models of the defects in $FeCl_2$. Large chlorine ions may not change the nearly close-

packed structure and only small iron atoms may change their positions or charges.

Fig.15. The absorption curve of Mn^{2+} spin resonances in $FeCl_2$ at 85 Gc/sec and 1.5°K. The left sharp line is the resonance absorption in antiferromagnetic state of $FeCl_2$ with increasing field, and the other two lines are the absorption in ferromagnetic state.

Fig.16. Concentration variation of absorption intensity at 1.5°K. wt.% is nearly equal to atmic % in these mixed crystals.

Fig.17. Frequency-field diagram of Mn^{2+} resonances. Solid lines are the theoretical lines corresponding to each state in Fig.19.

Fig.18. Temperature dependence of absorption intensity of Mn^{2+} resonance at 45 Gc/sec.

Fig.19. Spin arrangements of Mn^{2+} spin in $FeCl_2$.

Fig.20. Angular dependence of Mn^{2+} spin resonance points in antiferromatnetic state. Solid lines are the theoretical lines in accord with Eq.(16).

Fig.21. (a) A model of interstitial Fe^{3+} spin in $FeCl_2$.
(b) Simplified model of three spin system.
H_{E1} and H_{E2} include both the exchange and anisotropy field acting on S_1 and S_2, respectively.

Fig.22. Variation of effective g*-value with inclining the external field from the c-axis. Experimental points are reduced from Fig.12 and theoretical line is calculated taking $g_{//}=2.4$ and $g_{\perp}=10$.

Fig.23. Structures of resonance patterns of Mn^{2+}-Mn^{2+} pair at (a) 4.2°K and (b) 1.4°K and at 45 Gc/sec. Specimen contains 3.7 % Mn^{2+} impurities.

Fig.24. Temperature dependences of the absorption intensities of Mn^{2+}-Mn^{2+} pair resonance for 1.7 % Mn^{2+} specimen.

Fig.25. Frequency-field diagram of Mn^{2+}-Mn^{2+} pair resonance. Dotted lines are theoretical ones in accord with Eq.(23).

	θ (^{o}K)	$T_{\chi\ max}$ (^{o}K)	$T_{C_p\ max}$ (^{o}K)
$MnCl_2$	-3.3	--	1.96, 1.81
$FeCl_2$	48.0	24	23.5
$FeCl_3$	-11.5	--	?
$CoCl_2$	38.1	25	24.9
$NiCl_2$	68.2		49.6

The transition at 1.96^{o}K of $MnCl_2$ is from the paramagnetic state to the antiferromagnetic state and the transition at 1.81^{o}K is to a second antiferromagnetic modification.

Table 1

The transition temperatures of some anhydrous chlorides of iron group.

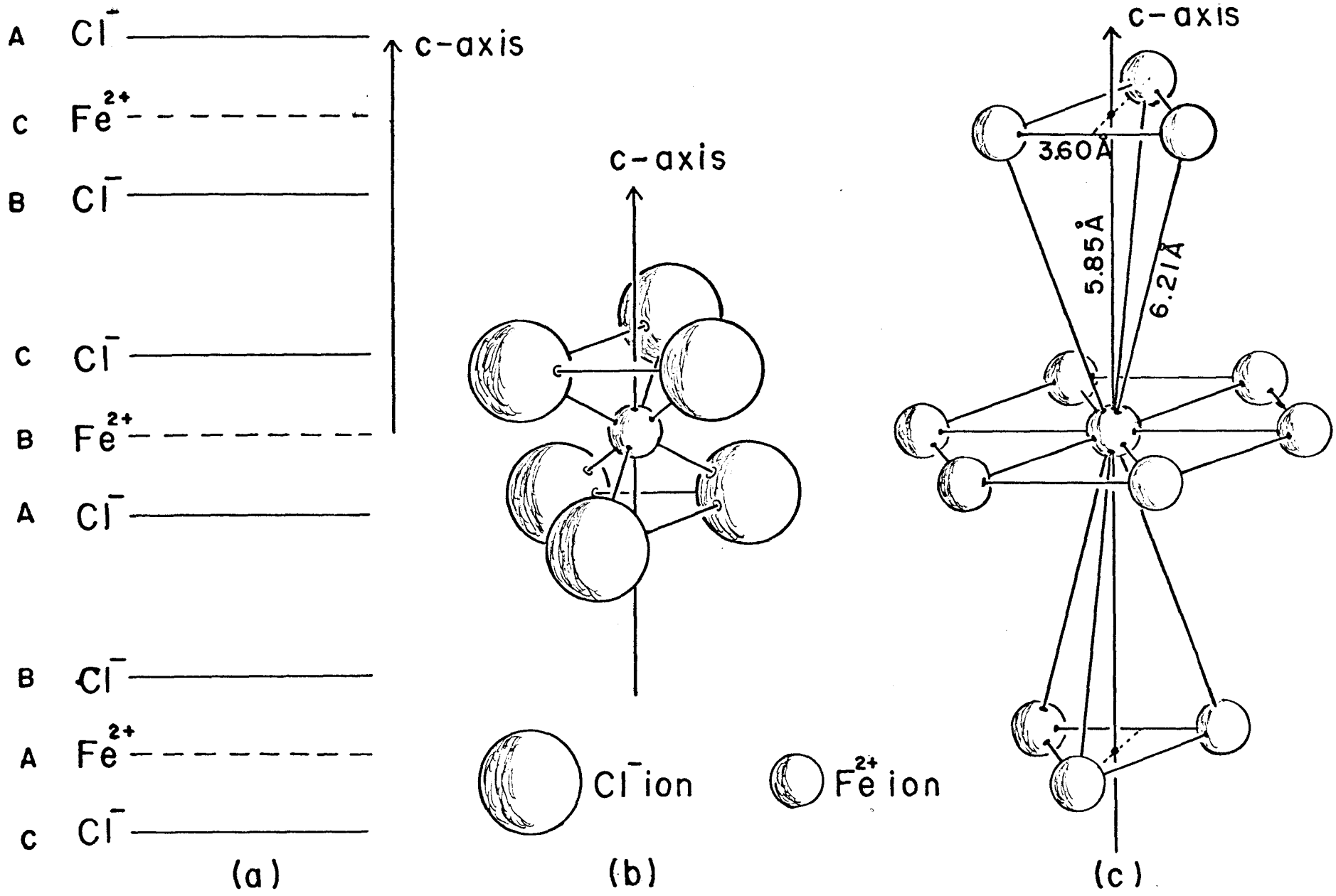

Fig. 1 Motokawa

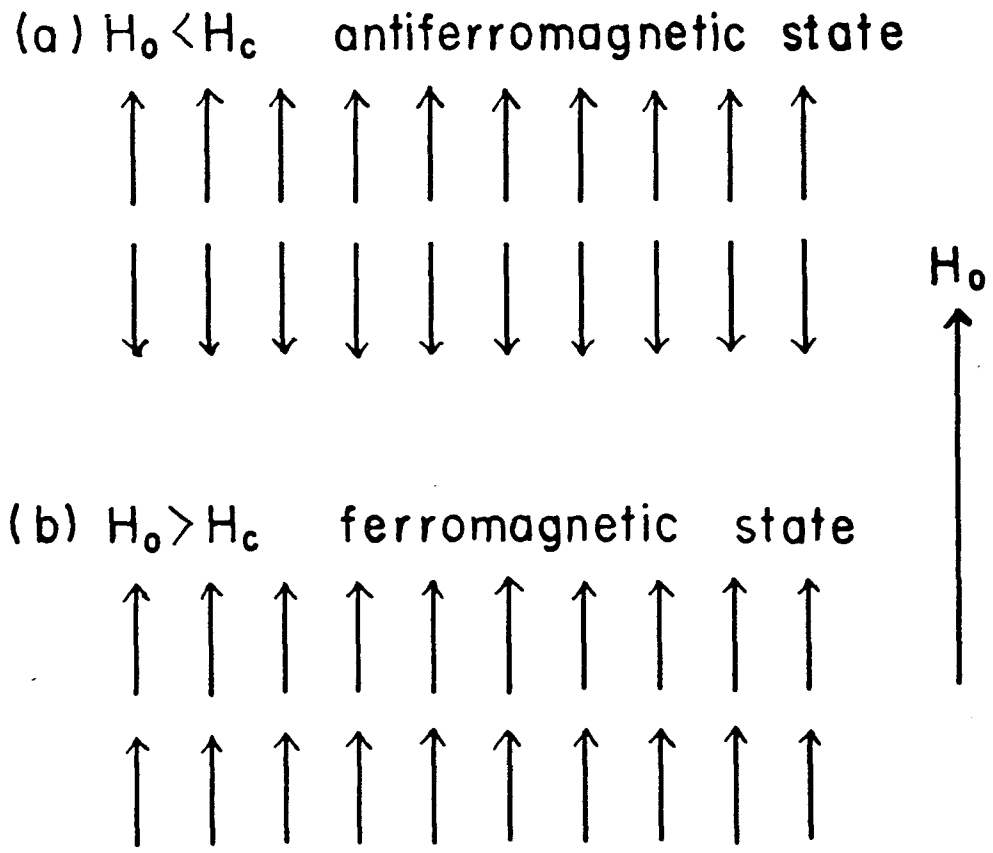

Fig. 2. Motokawa

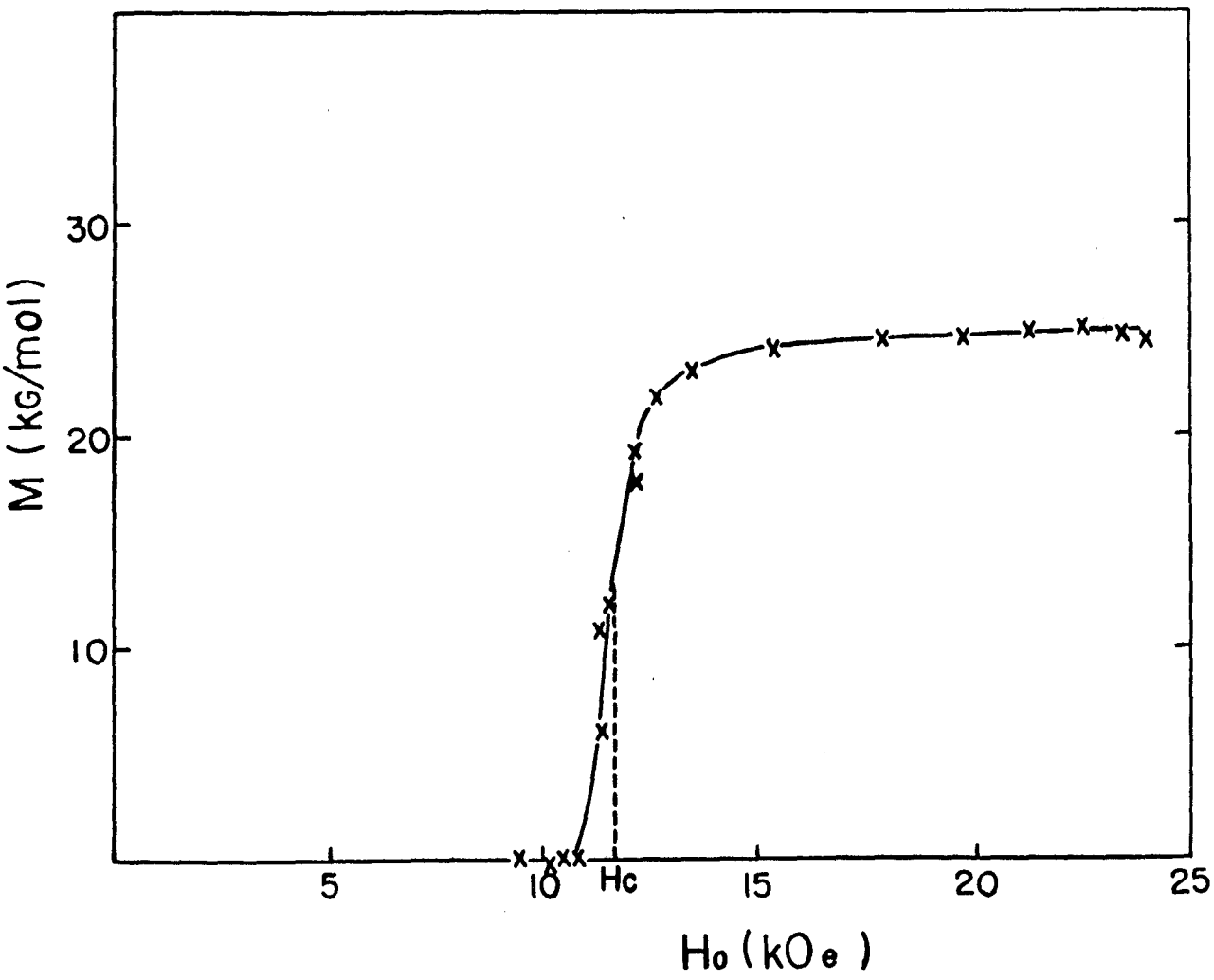

Fig. 3.

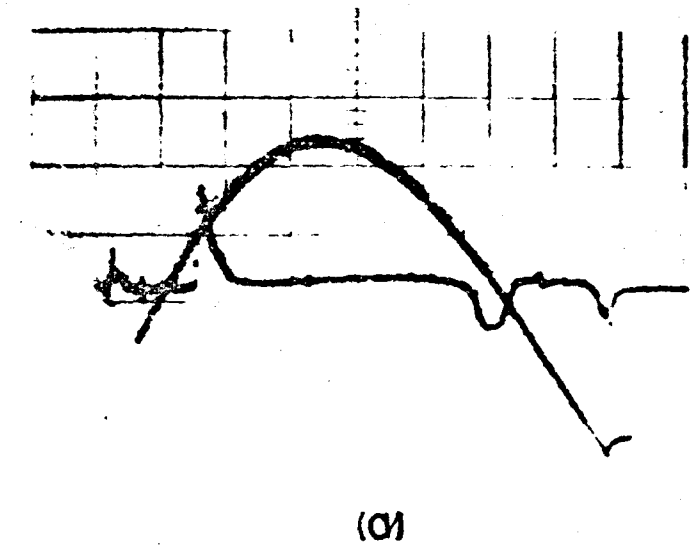

(a)

(b)

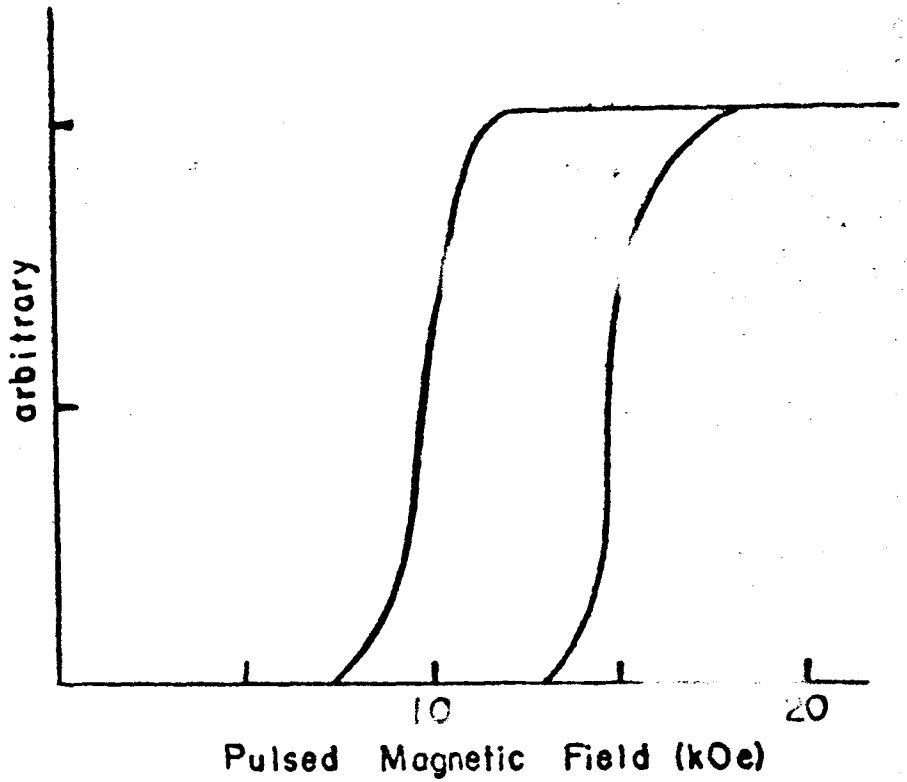

(c)

Fig. 4

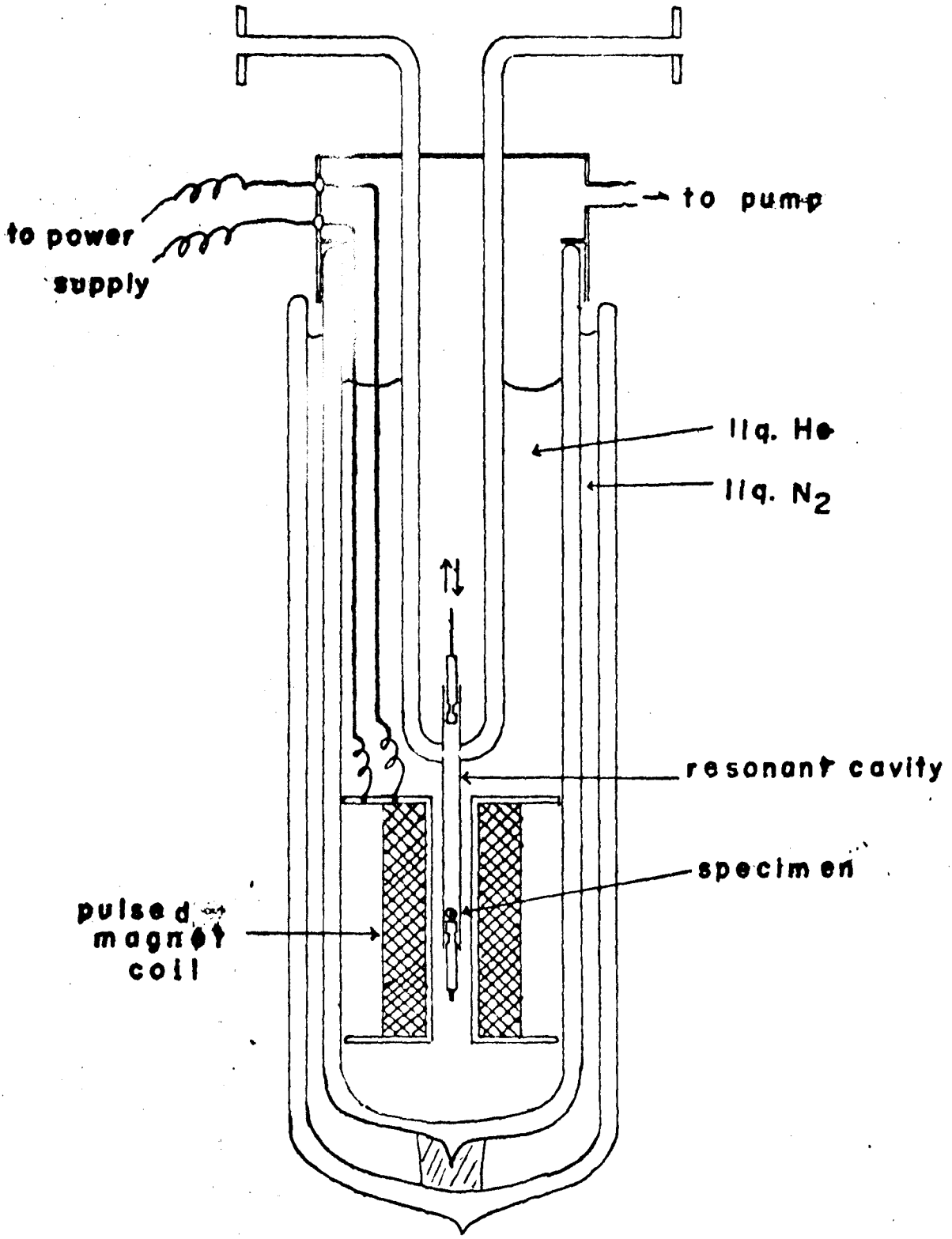
to power
supply
to pump
liq. He
liq. N_2
resonant cavity
specimen
pulsed
magnet
coil

Fig 5 Mahan

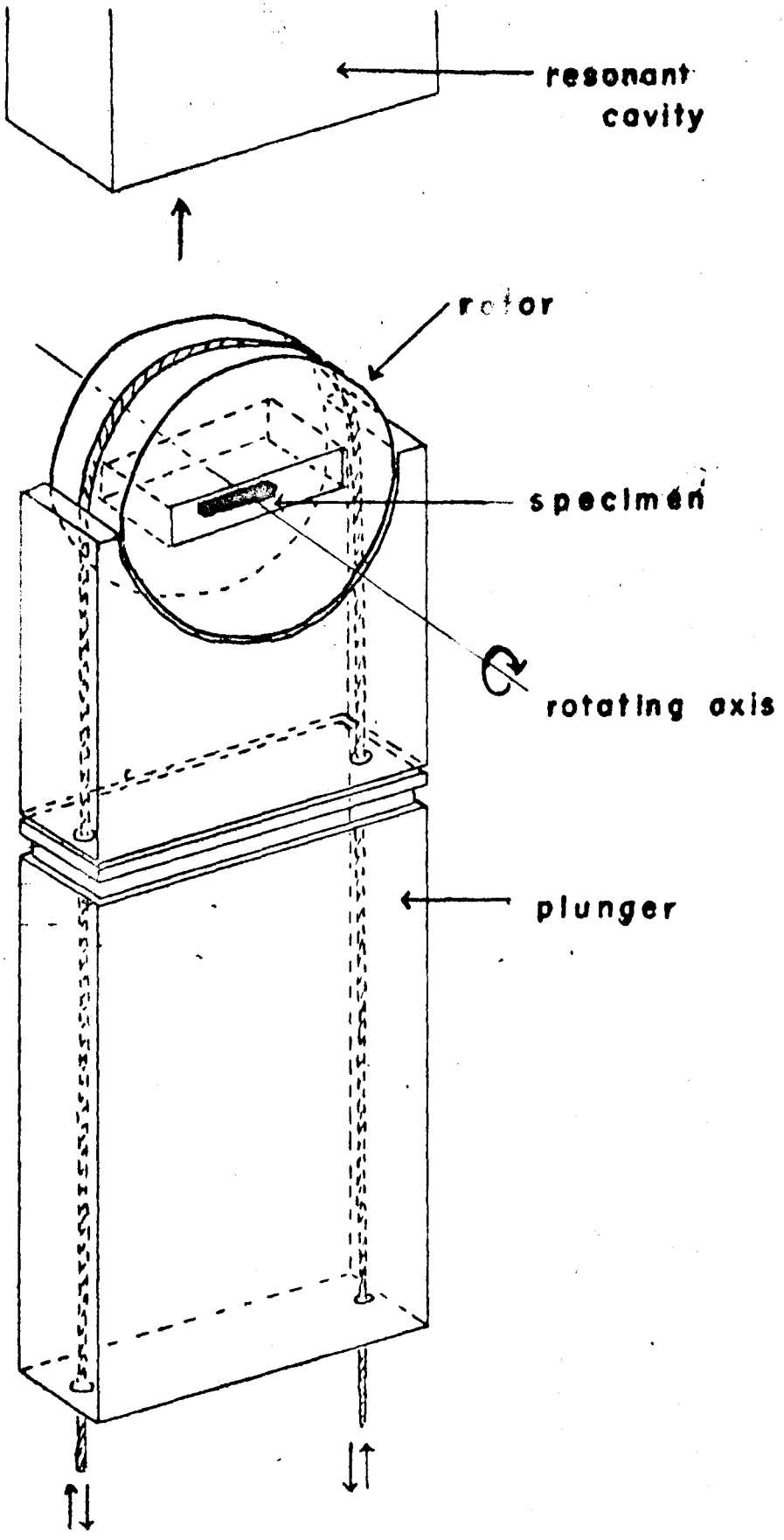

Fig. 6 Motokura

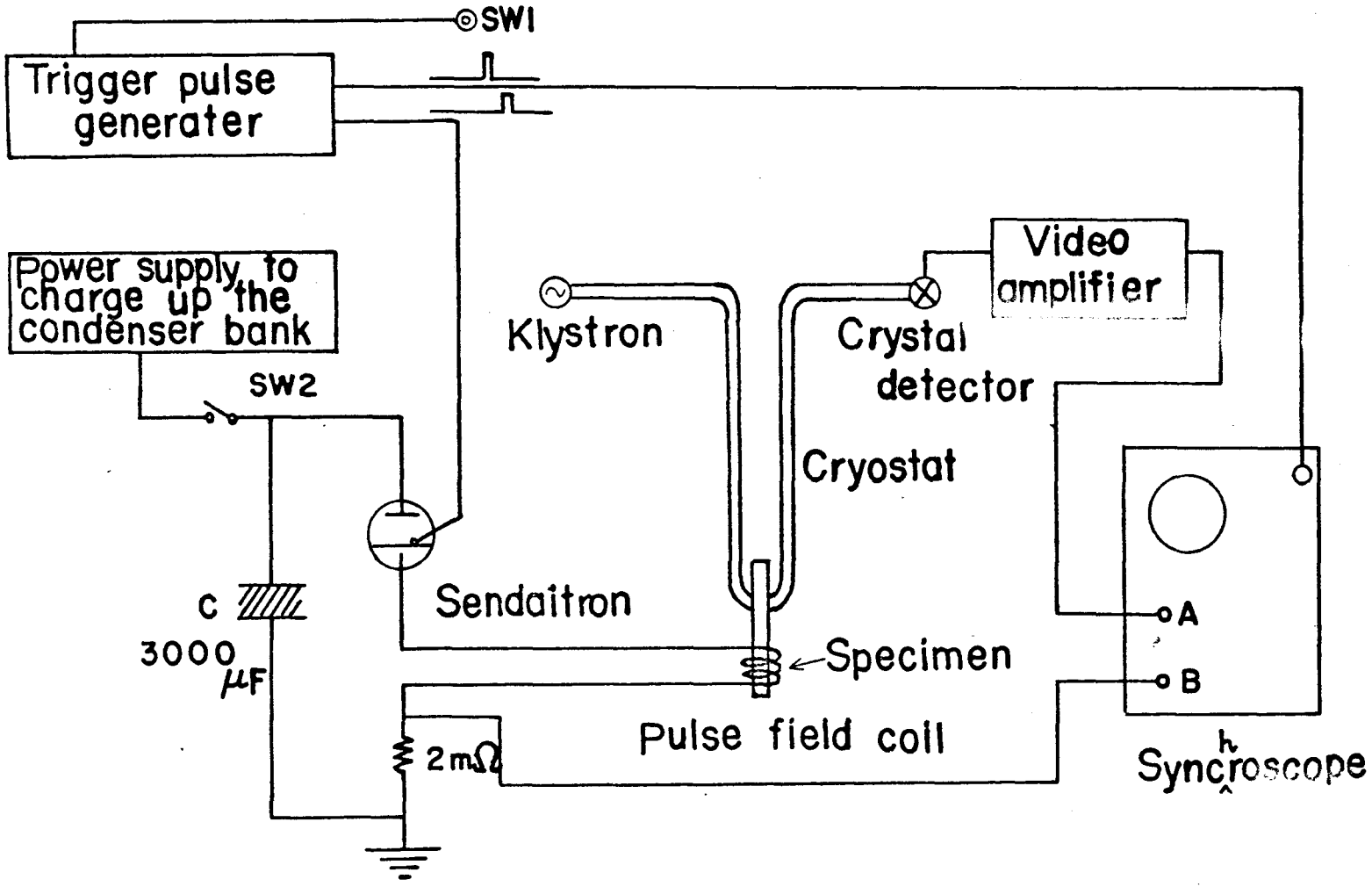

Fig. 7. Motokawa

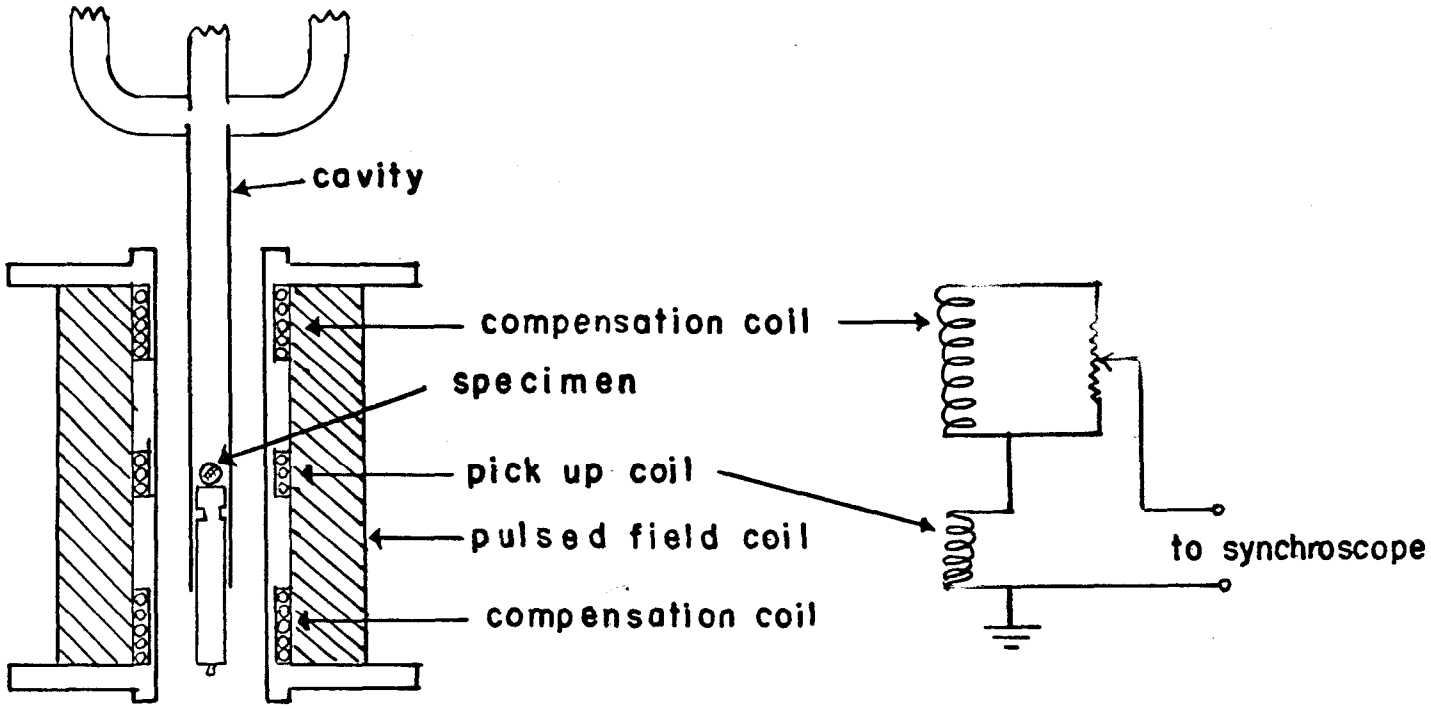

Fig. 8 Motokawa

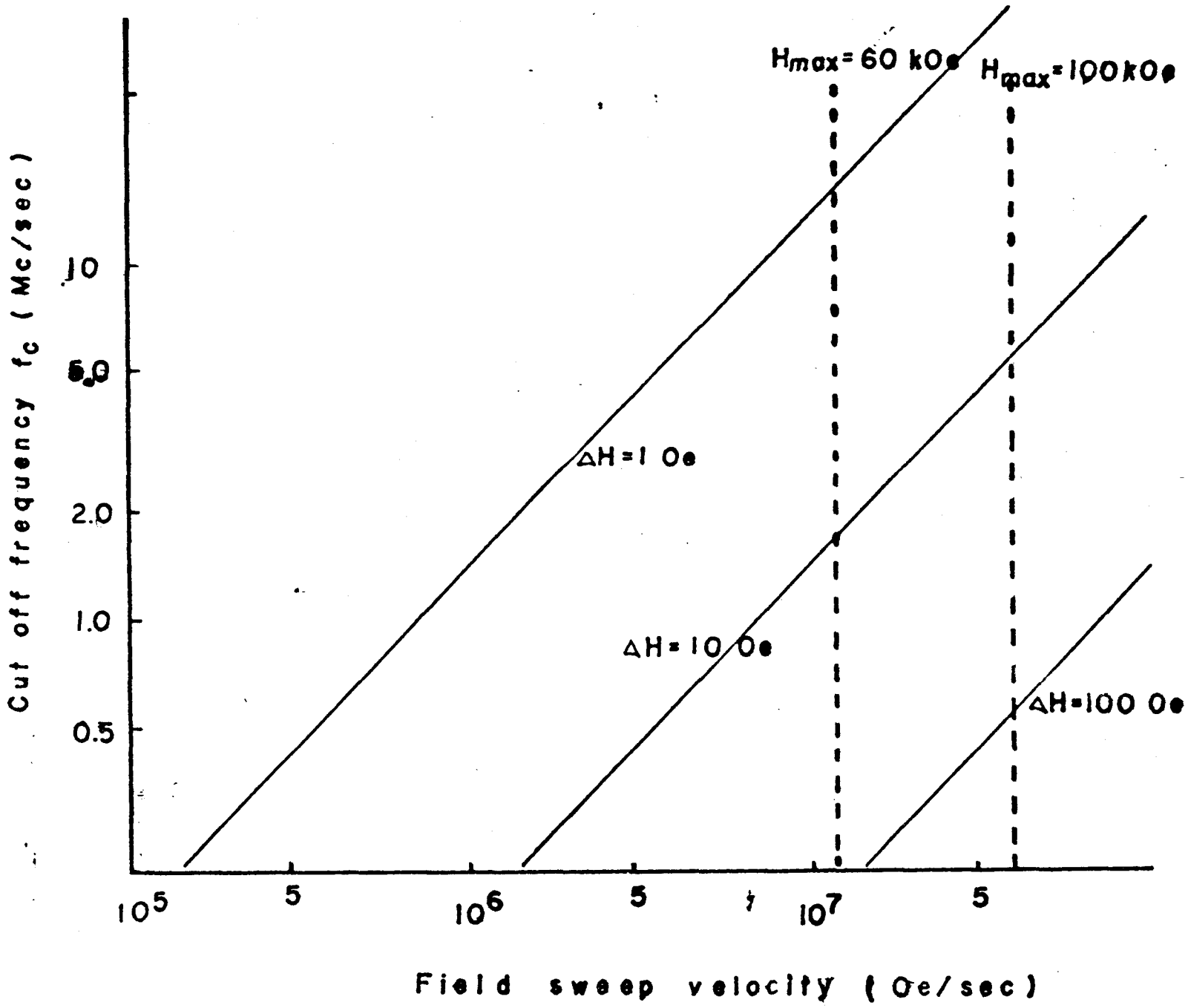
Hmax= 60 kOe
Hmax=100kOe
ΔH=1 Oe
ΔH=10 Oe
ΔH=100 Oe
Cut off frequency fc (Mc/sec)
10
5.0
2.0
1.0
0.5
10^5
5
10^6
5
10^7
5
Field sweep velocity (Oe/sec)

Fig. 9

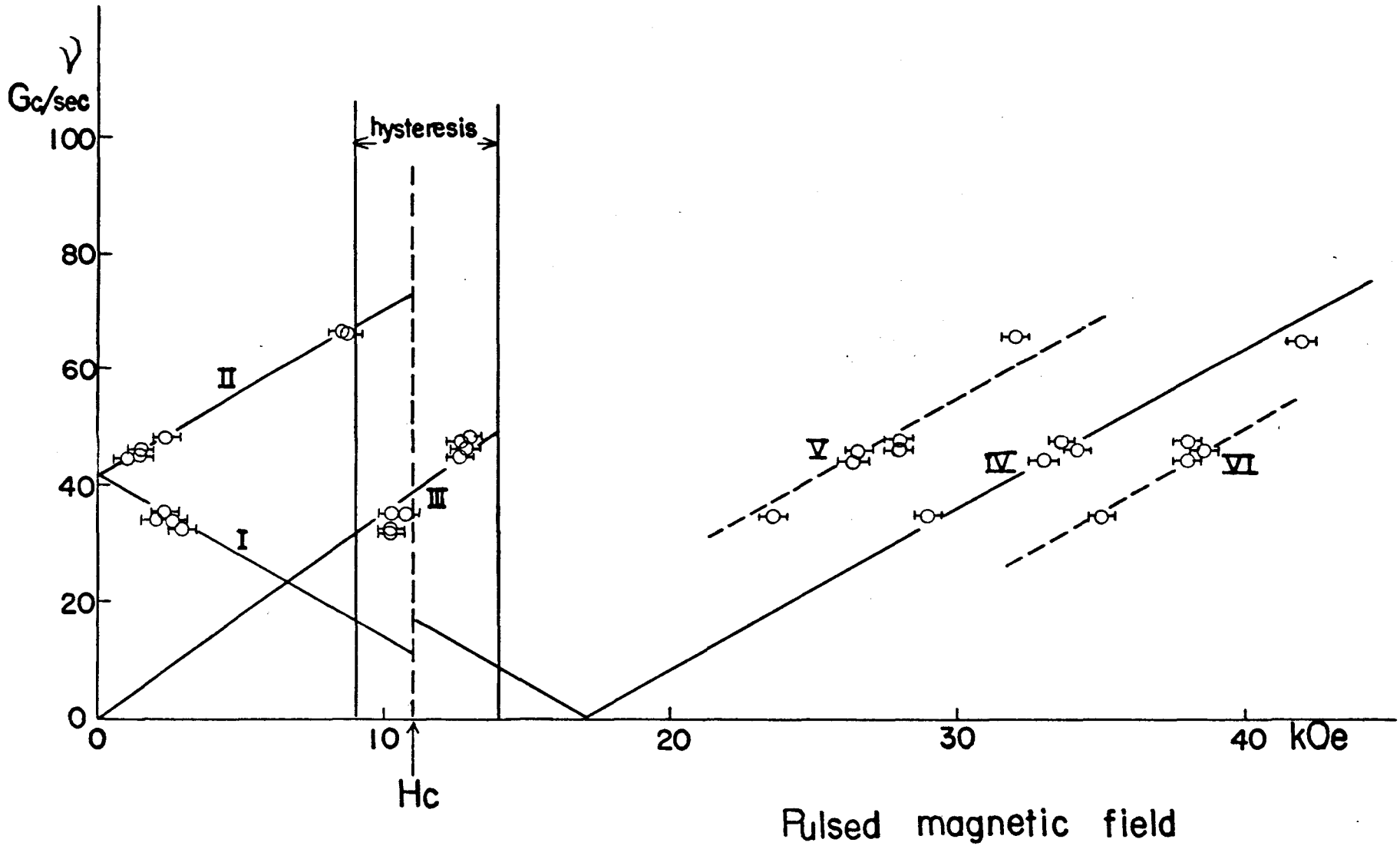
ν
Gc/sec
100
80
60
40
20
0
hysteresis
I
II
III
IV
V
VI
0
10
20
30
40 kOe
Hc
Pulsed magnetic field

Fig. 10

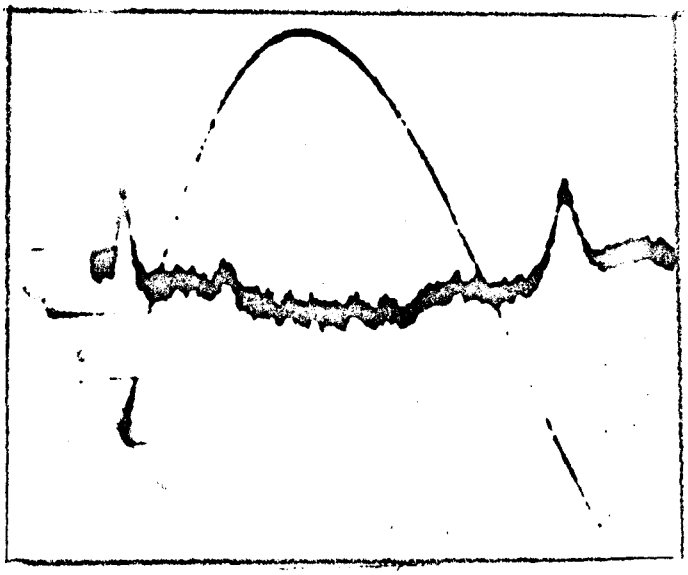

Fig. 11

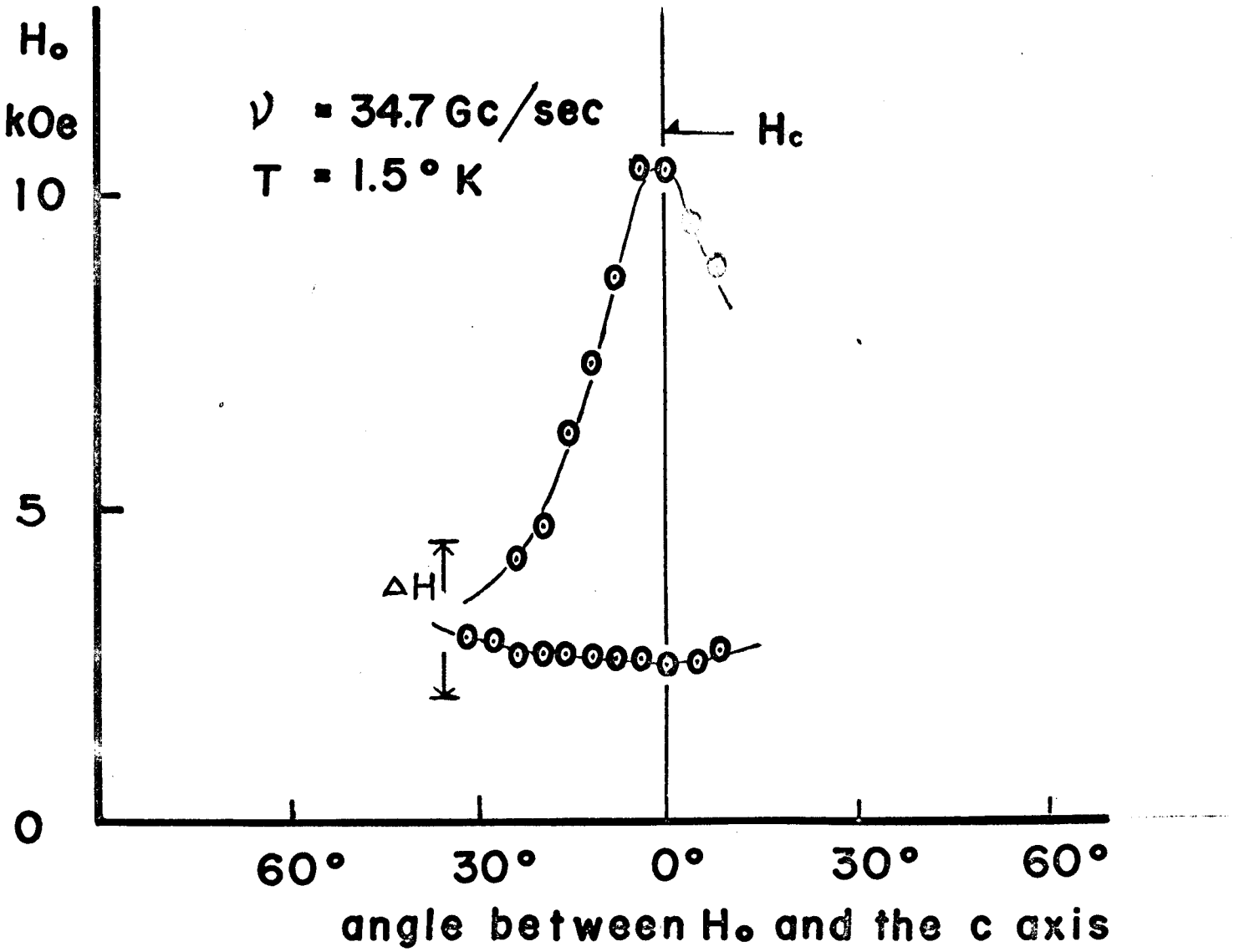
H_o
kOe
10
5
0
ν = 34.7 Gc/sec
T = 1.5° K
H_c
ΔH
60°
30°
0°
30°
60°
angle between H_o and the c axis

Fig. 12

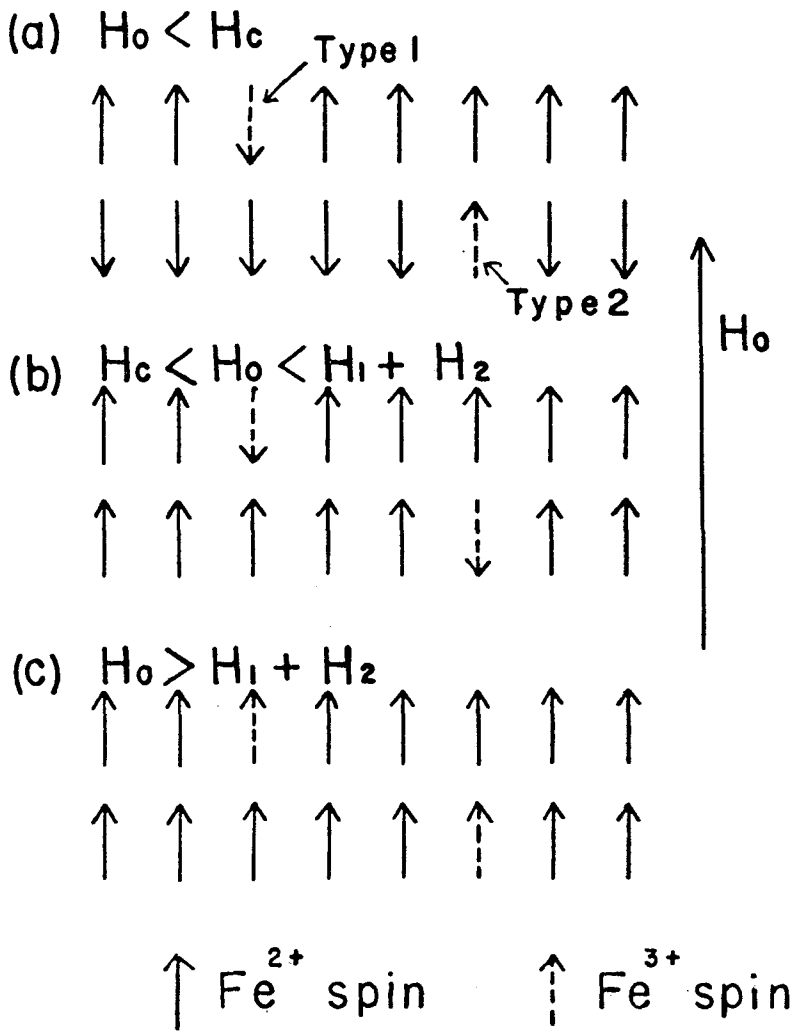

$$\omega/\gamma = H_1 - H_2 - H_0 \quad \text{I}$$

$$\omega/\gamma = H_1 - H_2 + H_0 \quad \text{II}$$

$$\omega/\gamma = H_1 + H_2 - H_0$$

$$\omega/\gamma = H_0 - (H_1 + H_2) \quad \text{IV}$$

Fig. 13

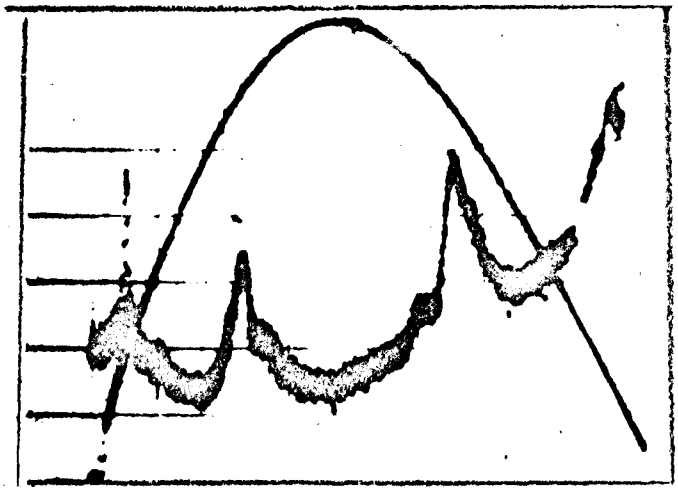

Fig. 15

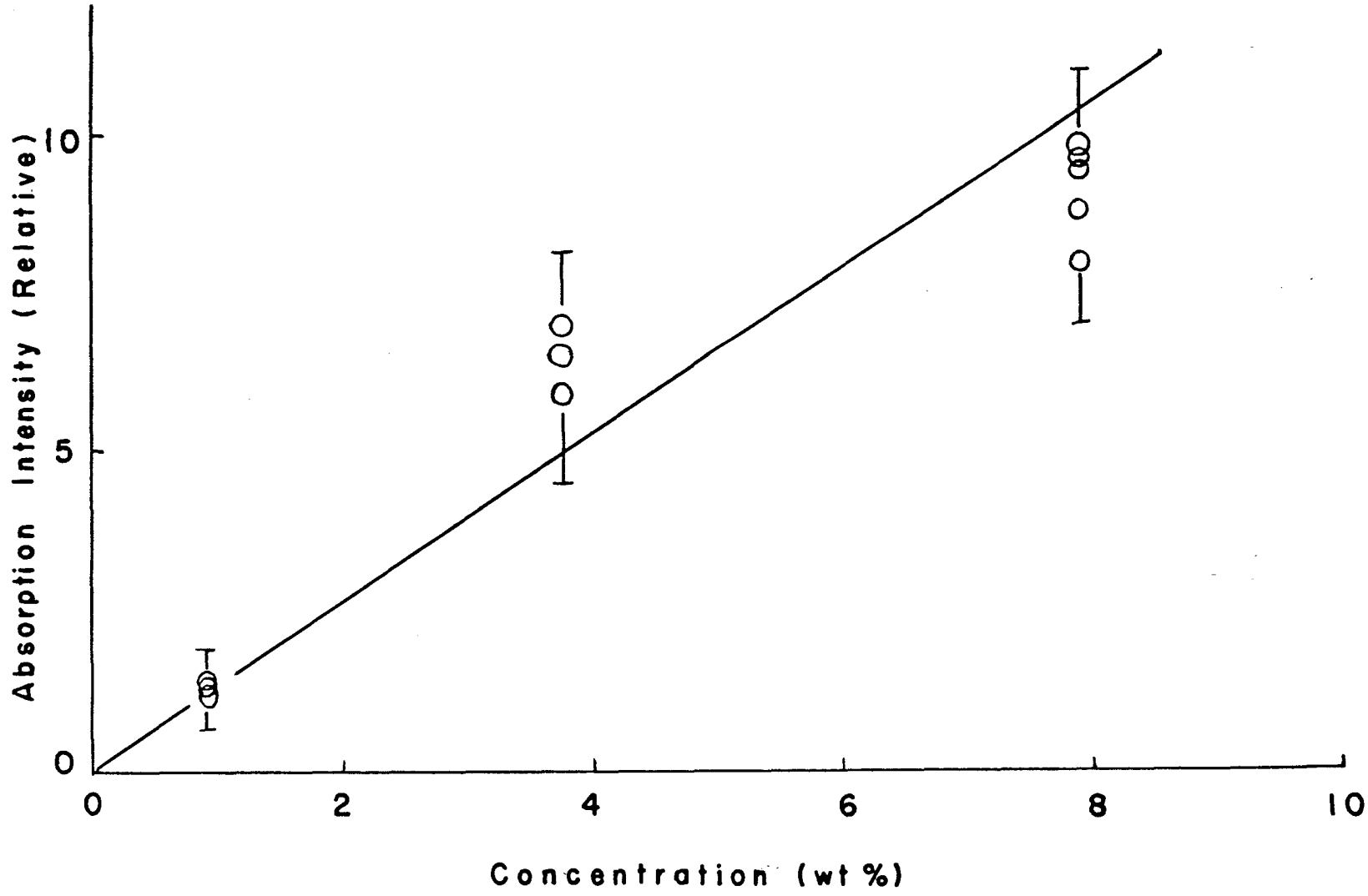
Absorption Intensity (Relative)
0
5
10
0
2
4
6
8
10
Concentration (wt %)

Fig. 16

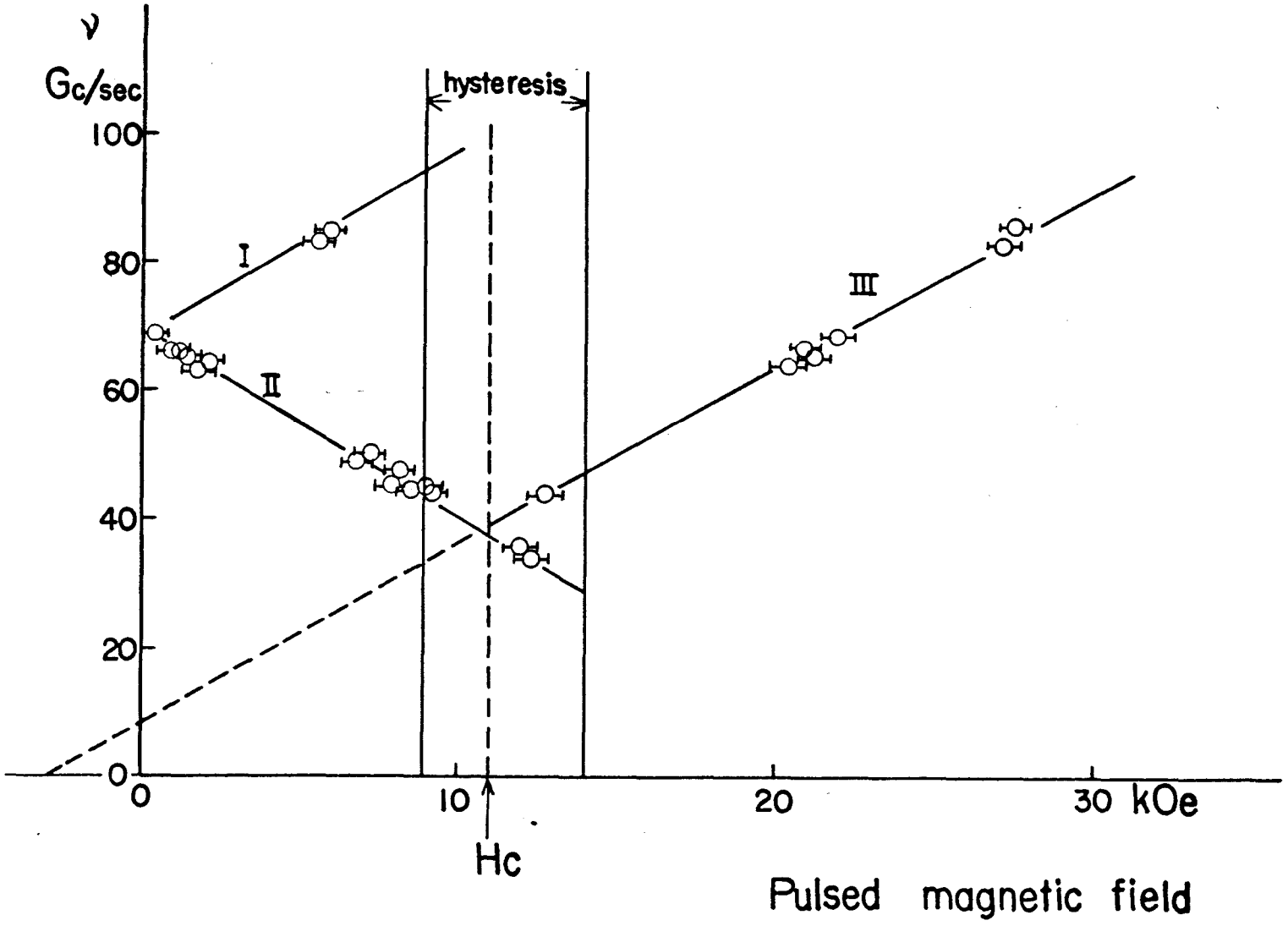
ν
Gc/sec
100
80
60
40
20
0
hysteresis
I
II
III
0
10
20
30 kOe
Hc
Pulsed magnetic field

Fig. 17

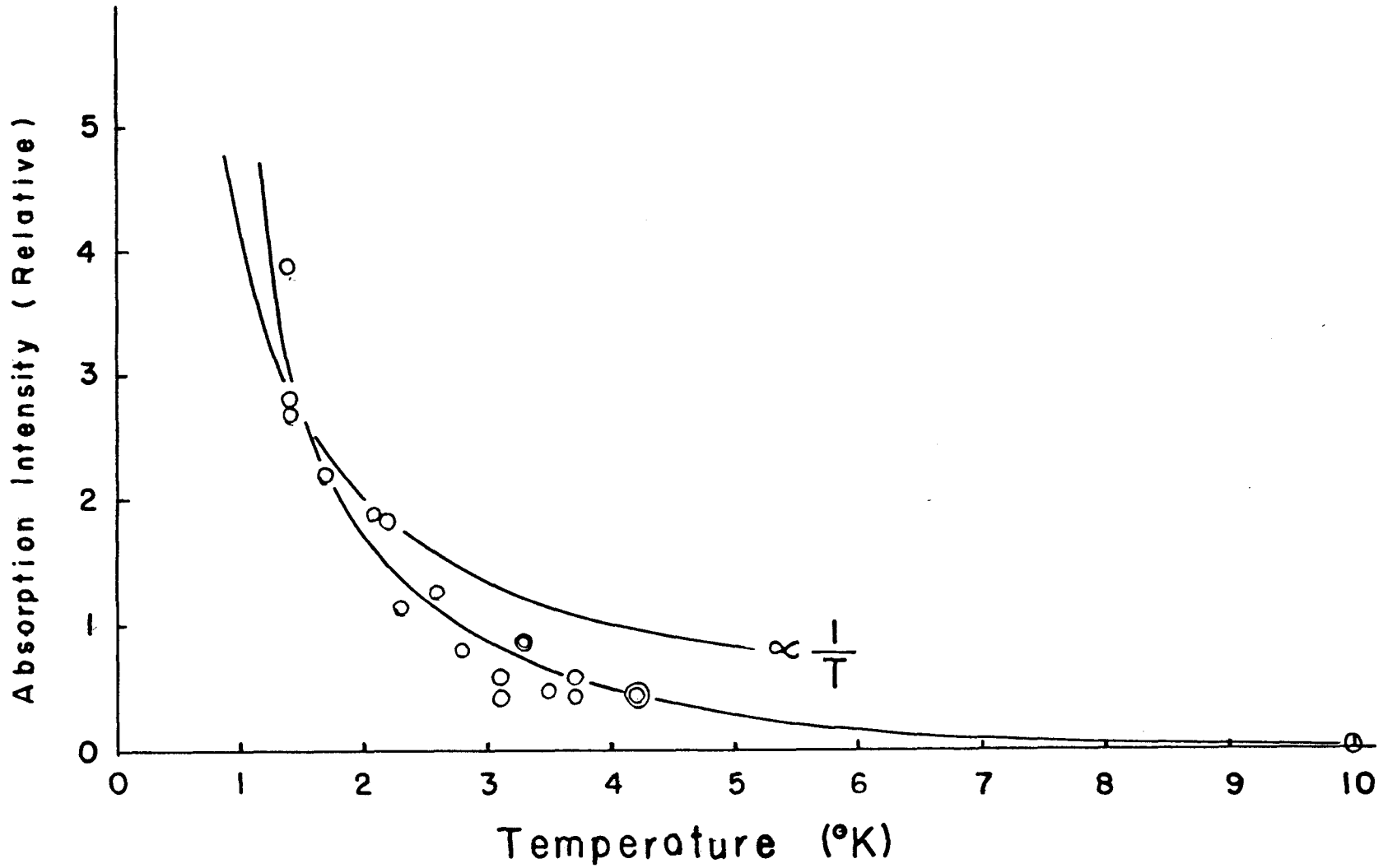
Absorption Intensity (Relative)
0
1
2
3
4
5
0
1
2
3
4
5
6
7
8
9
10
Temperature (°K)
∝ 1/T

Fig. 18

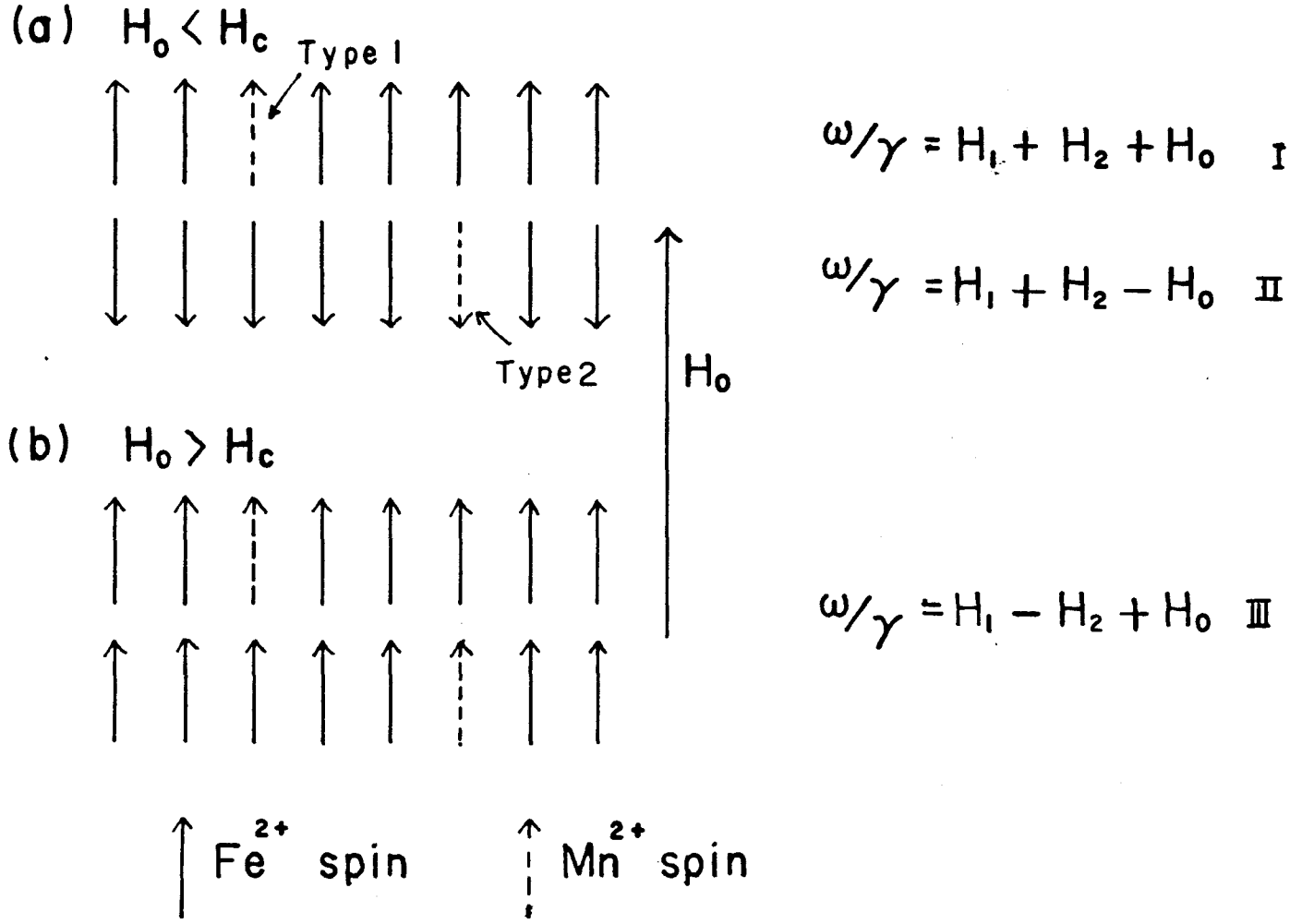
(a) $H_0 < H_c$
Type 1
Type 2
H_0
(b) $H_0 > H_c$
Fe^{2+} spin
Mn^{2+} spin
$\omega/\gamma = H_1 + H_2 + H_0$ I
$\omega/\gamma = H_1 + H_2 - H_0$ II
$\omega/\gamma = H_1 - H_2 + H_0$ III

Fig. 19

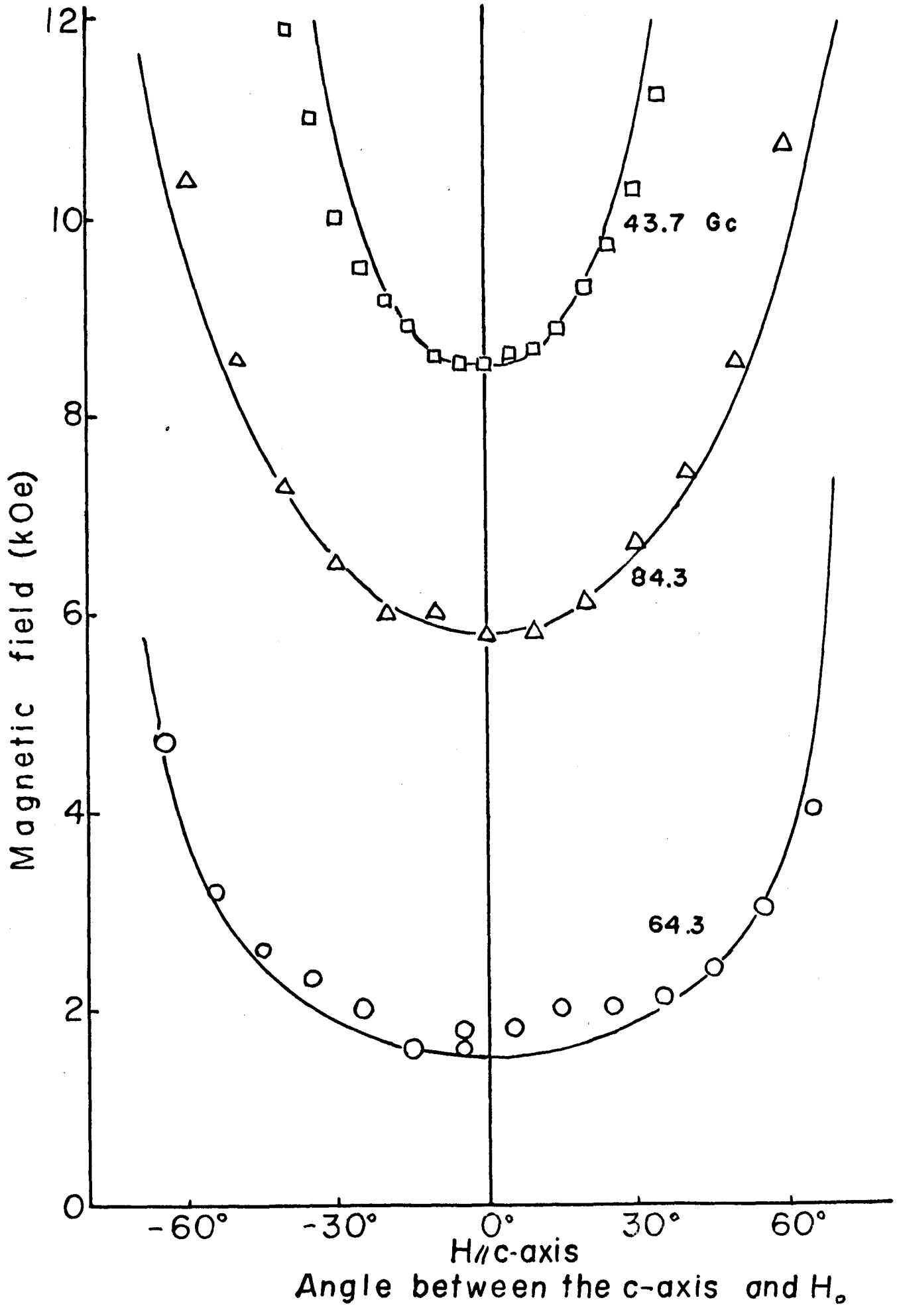
12
10
8
6
4
2
0
Magnetic field (kOe)
43.7 Gc
84.3
64.3
-60°
-30°
0°
30°
60°
H//c-axis
Angle between the c-axis and H₀

Fig. 20

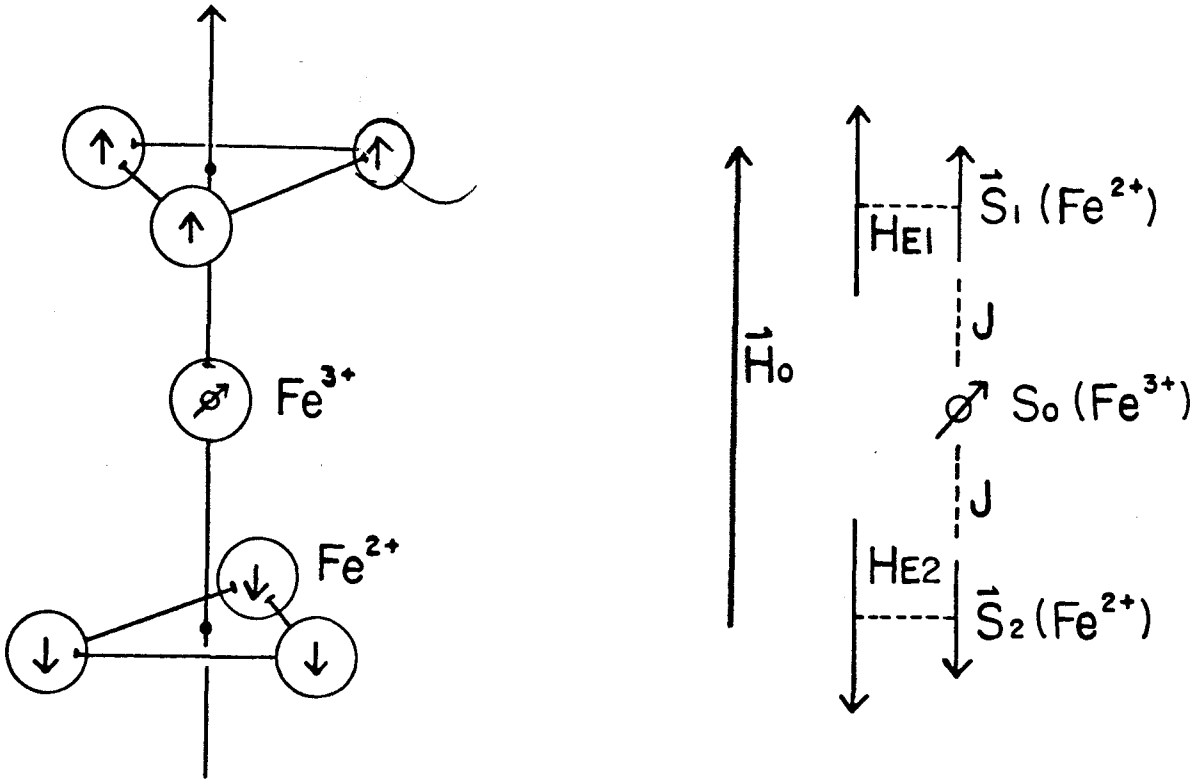

Fig. 21

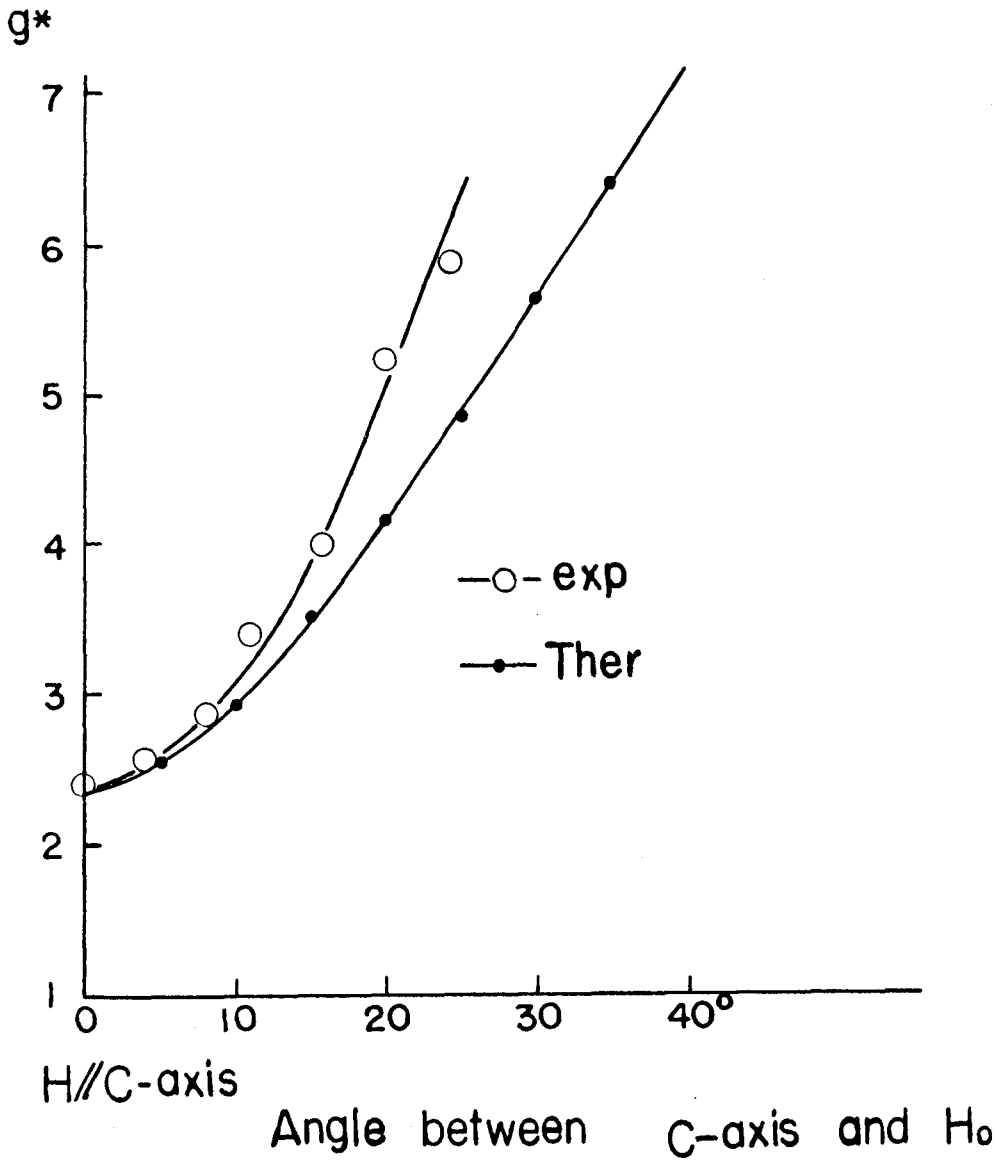
g*
7
6
5
4
3
2
1
0
10
20
30
40°
—○— exp
—●— Ther
H//C-axis
Angle between C-axis and Ho

Fig. 22

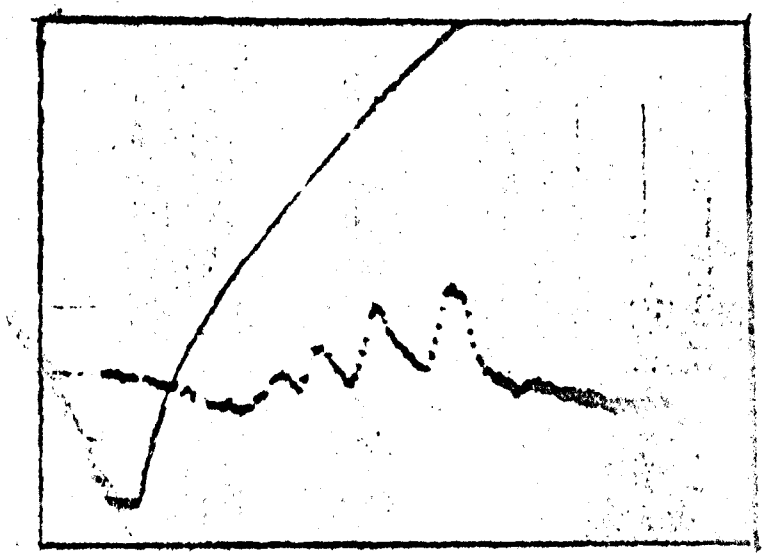

(a)

(b)

Fig 23

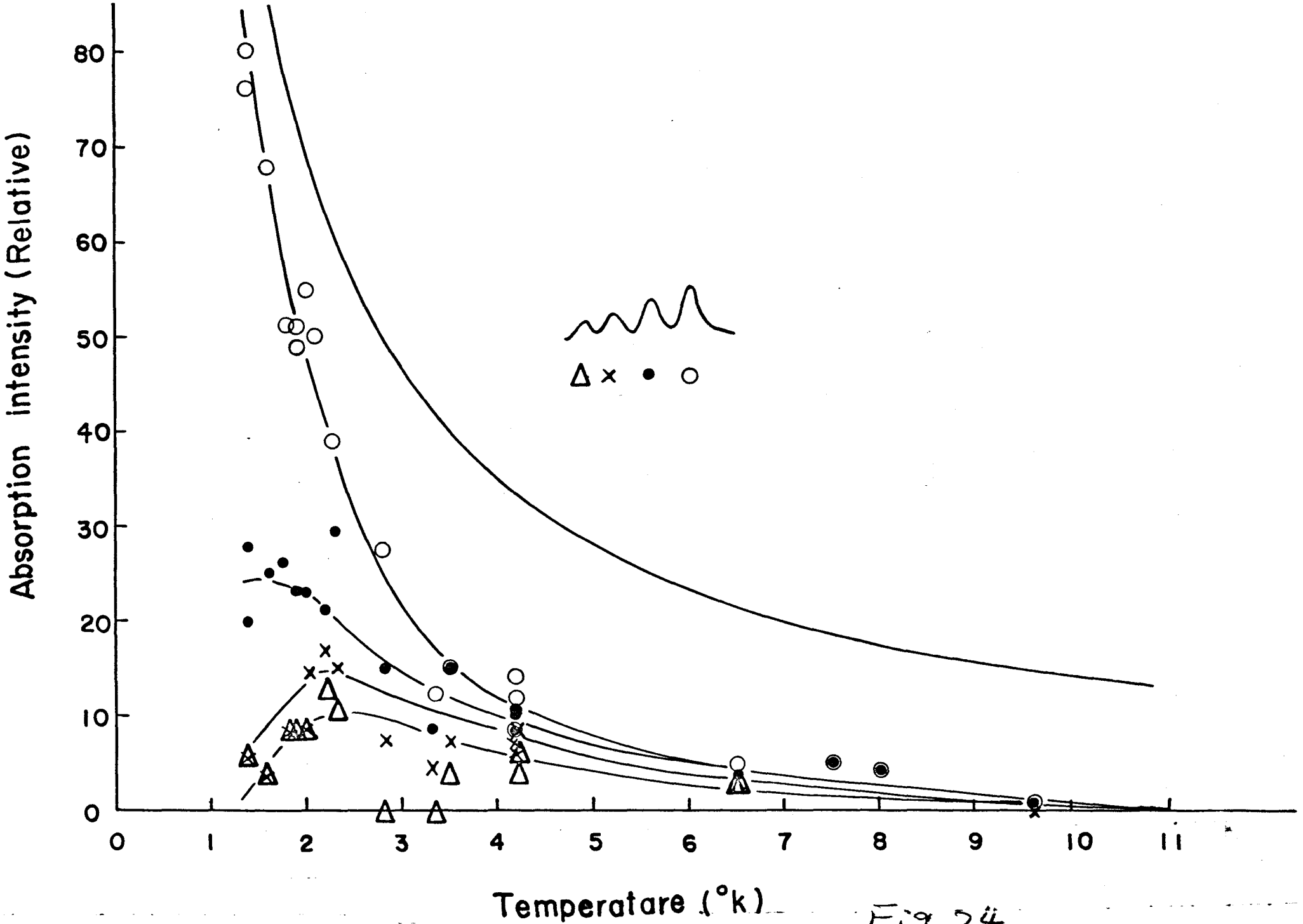
Absorption Intensity (Relative)
80
70
60
50
40
30
20
10
0
0
1
2
3
4
5
6
7
8
9
10
11
Temperatare (°k)
Δ × • ○

Fig. 24

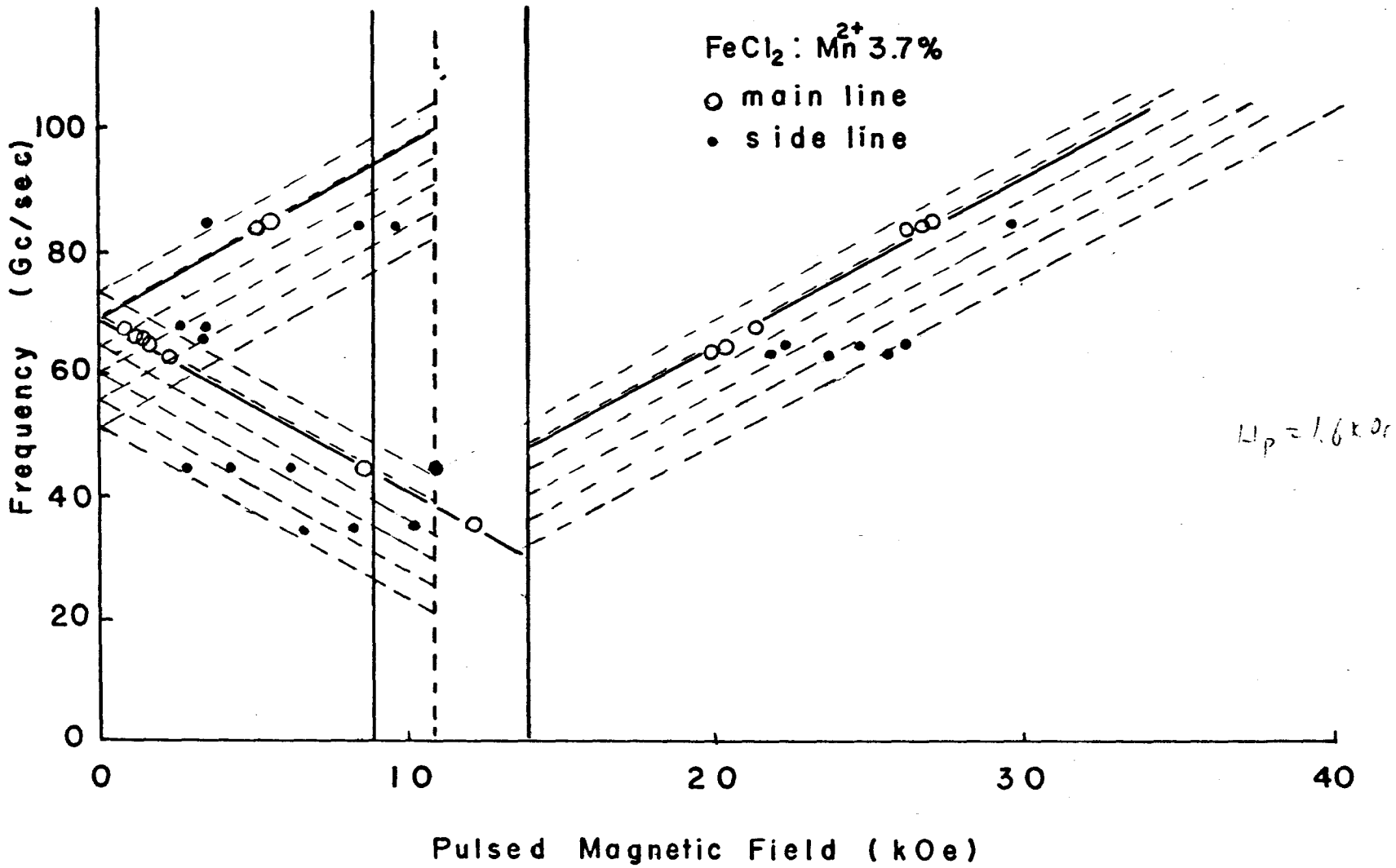
FeCl2 : Mn2+ 3.7%
o main line
• side line
Frequency (Gc/sec)
100
80
60
40
20
0
0
10
20
30
40
Pulsed Magnetic Field (kOe)

Fig. 25